



HAL
open science

TLR or NOD receptor signaling skews monocyte fate decision via distinct mechanisms driven by mTOR and miR-155

Alice Coillard, Léa Guyonnet, Alba de Juan, Adeline Cros, Elodie Segura

► To cite this version:

Alice Coillard, Léa Guyonnet, Alba de Juan, Adeline Cros, Elodie Segura. TLR or NOD receptor signaling skews monocyte fate decision via distinct mechanisms driven by mTOR and miR-155. Proceedings of the National Academy of Sciences of the United States of America, 2021, 118 (43), pp.e2109225118. 10.1073/pnas.2109225118 . inserm-03420662

HAL Id: inserm-03420662

<https://inserm.hal.science/inserm-03420662>

Submitted on 9 Nov 2021

HAL is a multi-disciplinary open access archive for the deposit and dissemination of scientific research documents, whether they are published or not. The documents may come from teaching and research institutions in France or abroad, or from public or private research centers.

L'archive ouverte pluridisciplinaire **HAL**, est destinée au dépôt et à la diffusion de documents scientifiques de niveau recherche, publiés ou non, émanant des établissements d'enseignement et de recherche français ou étrangers, des laboratoires publics ou privés.

TLR or NOD receptor signaling skews monocyte fate decision via distinct mechanisms driven by mTOR and miR-155

Alice Coillard^{1,2}, Léa Guyonnet³, Alba De Juan¹, Adeline Cros¹ and Elodie Segura^{1*}

¹ Institut Curie, PSL Research University, INSERM, U932, 26 rue d'Ulm, 75005 Paris, France

² Université Paris Descartes, Paris, France

³ Institut Curie, PSL Research University, Flow Cytometry Core, 26 rue d'Ulm, 75005 Paris, France

* Correspondence:

Elodie Segura

elodie.segura@curie.fr

Abstract

Monocytes are rapidly recruited to inflamed tissues where they differentiate into monocyte-derived macrophages (mo-mac) or dendritic cells (mo-DC). At infection sites, monocytes encounter a broad range of microbial motifs. How pathogen recognition impacts monocyte fate decision is unclear. Here we show, using an *in vitro* model allowing the simultaneous differentiation of human mo-mac and mo-DC, that viruses promote mo-mac while mycobacteria favor mo-DC differentiation. Mechanistically, we found that pathogen sensing through TLR ligands increases mo-mac differentiation via mTORC1. By contrast, NOD ligands favor mo-DC through the induction of TNF- α secretion and miR-155 expression. We confirmed these results *in vivo*, in mouse skin and by analyzing transcriptomic data from human individuals. Overall, our findings allow a better understanding of the molecular control of monocyte differentiation, and of monocyte plasticity upon pathogen sensing.

Classification: Biological Sciences/Immunology and Inflammation

Keywords: Monocyte; Macrophage; Dendritic cell; Pathogen

Significance Statement

Monocytes are key players in immune responses to pathogen entry. They exert a major part of their function through their differentiation into macrophages or dendritic cells, two populations with largely distinct roles in immune responses. Yet, we still have a very limited view of the factors orientating monocyte fate to become macrophages versus dendritic cells, in particular how pathogen recognition modulates this process. Here we show that pathogen sensing skews monocyte fate decision, i.e. the first steps of the differentiation process, with TLR signaling favoring macrophage development while NOD receptor signaling induces dendritic cell differentiation.

Introduction

Immune defense against microbial infections critically relies on the rapid mobilization of professional phagocytes, in particular macrophages and monocytes. Upon pathogen recognition, they increase their ability to engulf dying cells and produce antimicrobial molecules to control the infection. In addition, microbe sensing reprograms macrophages towards a pro-inflammatory state (1). However, how pathogen-derived products impact monocyte fate remains unclear.

Monocytes originate from the bone marrow and are massively recruited in tissues upon infection (2). They play an essential role in the control of infections as shown in CCR2-deficient mice, in which monocytes are unable to exit the bone marrow to circulate in the bloodstream (3, 4). In models of bacterial or viral infections, CCR2-deficient mice display higher bacterial or viral loads and lower survival (5–8). In addition to their immediate action in pathogen elimination, monocytes are involved in the immune response against infections through their capacity to differentiate into monocyte-derived macrophages (mo-mac) and monocyte-derived dendritic cells (mo-DC) (9, 10). Mo-mac can replace tissue-resident macrophages that have died upon infection (11, 12), or retain increased reactivity to subsequent inflammation (13, 14). Mo-DC can complement the action of classical DC in the induction of adaptive responses, by presenting antigens to T cells directly in tissues to boost their effector functions (15–17). On the other hand, dysregulated monocyte recruitment and/or differentiation during infections can lead to increased tissue damage, high pathogen burden and mortality (18–20). A tight control of these events therefore appears critical for mounting efficient immune responses. Yet, the factors regulating monocyte fate decision are poorly understood both at the molecular level and in a broader physiological context. *In vivo* differentiation of monocytes is dependent on the M-CSF receptor (21). We have shown that circulating monocytes are not pre-committed to become mo-mac or mo-DC, and that their fate is driven by microenvironmental cues (22). Consistent with this, sterile inflammation accelerates monocyte differentiation in the intestine in mice (23). However, how pathogen recognition impacts monocyte fate decision remains unknown.

Using an *in vitro* model of human monocyte differentiation, we show that pathogen recognition through TLR promotes mo-mac differentiation *via* the mTORC1 pathway which increases MAFB expression. By contrast, NOD receptor activation favors mo-DC development through the autocrine action of TNF- α . We confirm these findings *in*

vivo in a mouse model and in humans using GSEA analysis of skin biopsies from individuals infected with HSV2 virus or joint biopsies from rheumatoid arthritis patients. Our results demonstrate that pathogen recognition skews monocyte fate decision, resulting in opposite outcomes depending on the nature of the pathogen.

Results

Exposure to viruses or Mycobacteria has opposite effects on monocyte differentiation

To address the impact of pathogen recognition on monocyte differentiation, we used our previously published *in vitro* model allowing the simultaneous differentiation of mo-mac and mo-DC (22). In this model, human monocytes cultured for 5 days with M-CSF, IL-4 and TNF- α differentiate into mo-mac (CD16+), mo-DC (CD1a+) or remain undifferentiated (double negative cells) (Fig. 1A). At the start of the culture, we exposed monocytes to inactivated or live virus, or heat killed Mycobacteria, and assessed their differentiation after 5 days. When exposed to inactivated Influenza A virus or live Sendai Virus, monocytes preferentially differentiated into mo-mac, while mo-DC differentiation was almost abrogated (Fig. 1B, Fig. 1C). By contrast, *Mycobacterium butyricum* (MB) significantly increased mo-DC differentiation (Fig. 1D). These results show that pathogen exposure impacts monocyte differentiation, with different outcomes depending on the pathogen. Mycobacteria contain motifs recognized by TLR and NOD receptors, which have been shown to antagonize each other (24, 25). To address whether NOD signaling was dominant in the observed effect on monocyte differentiation, we used GSK583, a chemical inhibitor of Receptor-interacting-serine/threonine-protein kinase 2 (RIPK2), the adapter protein required for NOD signal transduction. GSK583 inhibited the secretion by monocytes of IL-6 and IL-8 after exposure to the synthetic NOD2 ligand Murabutide, confirming the efficiency of this inhibitor (Fig. S1A). Enhanced mo-DC differentiation induced by heat-killed *Mycobacterium tuberculosis* (MT) was abrogated in the presence of GSK583 (Fig. 1E), indicating that Mycobacteria promote mo-DC through NOD signaling.

TLR ligands promote mo-mac differentiation while NOD ligands induce mo-DC

To decipher the molecular mechanisms involved, we used a reductionist approach and exposed monocytes to single ligands at the start of the culture, and assessed

their differentiation after 5 days (Fig. 2A). We found that monocytes exposed to Pam3 (TLR2 ligand, Fig. 2B, Fig. S1B), Gardiquimod (TLR7 ligand, Fig. 2C, Fig. S1B), LPS (TLR4 ligand, Fig. 2D, Fig. S1B) and R848 (TLR7/8 ligand, Fig. S1C) preferentially differentiated into mo-mac compared to the control condition. Gardiquimod and R848 also decreased the proportion of mo-DC, while Pam3 and LPS had no significant impact on mo-DC differentiation. By contrast, Murabutide (NOD2 ligand, Fig. 2E, Fig. S1B) and TriDAP (NOD1 ligand, Fig. 2F, Fig. S1B) promoted mo-DC differentiation without affecting the proportion of mo-mac. All these ligands activated monocytes to a similar extent, as shown by inflammatory cytokine secretion after 24h (Fig. S1D). In addition, TLR and NOD receptor ligands did not decrease either the percentage of live cells after 24 hours (Fig. S1E) or the number of live cells after 5 days (Fig. S1F), suggesting that these molecules impact the differentiation of monocytes rather than their survival. Monocyte exposure to Pam3, Gardiquimod, Murabutide and TriDAP did not modify the phenotype of mo-mac or mo-DC (Fig. 2G, Fig. S1G). These results show that exposure to pathogen-derived products impacts monocyte fate decision, with TLR ligands and NOD activation having opposite effects.

Monocyte exposure to TLR and NOD receptor ligands modifies the functional properties of mo-mac and mo-DC

We then addressed whether pathogen recognition by monocytes affects the functional properties of resulting mo-mac and mo-DC. We cell-sorted mo-mac and mo-DC differentiated from monocytes exposed or not to Pam3 or Murabutide, and assessed their capacity to secrete cytokines following stimulation, to induce T cell proliferation and polarization, and to perform phagocytosis (Fig. 3A). We first analyzed cytokine secretion by mo-DC and mo-mac. We measured the secretion of TNF- α , IL-6 and IL-8 after 24h of stimulation with Pam3, LPS, R848 or Murabutide (Fig. 3B). Mo-DC that differentiated from monocytes exposed to Pam3 or Murabutide secreted lower amounts of TNF- α , IL-6 and IL-8 following stimulation. Similar results were observed for mo-mac (Fig. 3B). To assess the ability of mo-DC and mo-mac to induce T cell proliferation and polarization, we performed a mixed leukocyte reaction with sorted mo-mac or mo-DC and allogeneic blood CD4 T cells. Mo-DC differentiated from monocytes exposed to Pam3 or Murabutide had a higher ability to stimulate naïve CD4 T cell proliferation compared to control mo-DC when using a low

number of antigen-presenting cells (Fig. 3C, Fig. S2A). By contrast, we did not find any significant difference for mo-DC in the induction of memory CD4 T cell proliferation (Fig. S2B). Mo-mac are poorer inducers of T cell proliferation as previously observed (22). Moreover, mo-mac differentiated from monocytes exposed to Pam3 or Murabutide had a lower capacity to induce naïve CD4 T cells proliferation (Fig. 3C, Fig. S2A). To analyze helper T cell polarization, we cultured isolated mo-DC and mo-mac with allogeneic blood naïve CD4 T cells for 6 days, and assessed cytokine production by T cells using intracellular flow cytometry. There was no major impact of monocyte exposure to pathogen products, except for Th2 polarization where mo-DC and mo-mac differentiated from monocytes exposed to Pam3 and Murabutide induced a lower proportion of IL-4-producing T cells (Fig. 3D). A higher expression of co-stimulatory molecules could explain the better ability of mo-DC differentiated from monocytes exposed to Pam3 and Murabutide to induce naïve CD4 T cell proliferation. However, we did not observe higher levels of CD80, CD86, HLADR or CD40 in comparison with control mo-DC or mo-mac (Fig. S2C). Finally, we assessed the phagocytic function of mo-DC and mo-mac. We performed a phagocytic assay using pHrodo green *S.aureus* bioparticles conjugate, which emits fluorescence only when exposed to an acidic pH in endocytic compartments. Mo-DC differentiated from monocytes exposed to Pam3 or Murabutide displayed lower phagocytic abilities compared to control mo-DC (Fig. 3E). We observed the same effect for mo-mac differentiated from monocytes exposed to Murabutide (Fig. 3E). Collectively, these results show that the functional properties of mo-mac and mo-DC are affected by pathogen recognition by progenitor monocytes, but independently of the nature of the pathogen compounds.

TLR ligands increase MAFB expression through mTORC1 activation

We have previously shown in this model that monocytes differentiate into mo-DC or mo-mac along two distinct pathways controlled by the transcription factors IRF4 and MAFB respectively (22). To elucidate the mechanisms involved in monocyte fate decision upon TLR ligand recognition, we first analyzed the impact of TLR ligands on *IRF4* and *MAFB* expression by RT-qPCR at early timepoints. Pam3 significantly decreased the expression of *IRF4* at 3h and 6h (Fig. 4A) and increased that of *MAFB* at 12 and 22h (Fig. 4B). To extend these observations to other TLR ligands, we repeated this analysis using Gardiquimod and LPS at relevant timepoints. Similar to

Pam3, Gardiquimod and LPS significantly decreased the early peak of *IRF4* expression (Fig. 4C). To test whether IRF4 and MAFB expression were modified at the protein level, we performed Western Blot analysis after 24h and 48h. Consistent with the RT-qPCR results, TLR ligands inhibited the expression of IRF4 protein (Fig. 4D). Moreover, Gardiquimod and LPS increased the expression of MAFB at the mRNA and protein levels to the same extent as Pam3 (Fig. 4E,F). These results indicate that exposure to TLR ligands strongly modifies the balance of IRF4 and MAFB expression by monocytes.

TLR signaling is known to induce mammalian target of rapamycin (mTOR) activation in immune cells (26, 27), and mTORC1 inhibition has been reported to promote mo-DC differentiation (28). Therefore we hypothesized that mTOR activation may impact monocyte differentiation upon TLR ligand exposure. To confirm that TLR ligands activate the mTOR pathway in human monocytes, we analyzed the phosphorylation of the ribosomal S6 protein, a surrogate of mTORC1 activation. Pam3 and Gardiquimod induced high amounts of ribosomal protein S6 phosphorylation (Fig. 4G-H). This effect was inhibited by the mTORC1 inhibitor Temsirolimus, confirming that this phosphorylation was dependent on mTORC1 (Fig. 4G-H). To address the impact of mTORC1 activation on *IRF4* and *MAFB* expression, we performed RT-qPCR on monocytes cultured in the presence or absence of Pam3 and Temsirolimus (Fig. 4I-J). mTORC1 inhibition had no significant impact on *IRF4* expression in the presence or absence of Pam3 (Fig. 4I). By contrast, the increase of *MAFB* expression induced by Pam3 was abrogated by the addition of Temsirolimus (Fig. 4J). These results show that TLR ligands increase MAFB expression through mTORC1 activation.

NOD receptor ligands promote mo-DC differentiation through TNF- α secretion

To understand how NOD receptor ligands induce mo-DC differentiation, we tested the hypothesis of a cell extrinsic mechanism relying on secreted factors. To this end, we performed supernatant transfer experiments (Fig. 5A). We stimulated or not monocytes with Murabutide for 30 minutes, then washed the cells and added fresh medium without Murabutide to obtain conditioned supernatant. After 1, 3 or 6 hours of incubation, we transferred this supernatant from the “supernatant donor” monocytes to unstimulated “supernatant recipient” monocytes from the same blood donor, and analyzed their differentiation after 5 days. As a control, we also cultured

the same monocytes without manipulating the medium (“untouched cells”), and confirmed that Murabutide exposure increased mo-DC differentiation in these cells (Fig. S3A). To test the potential carry-over of Murabutide in the conditioned medium, we measured the overnight secretion of IL-6 and IL-8 by the “supernatant recipient” monocytes that received the conditioned medium after 1h (Fig. S3B). There was no activation of monocytes in these conditions, showing that the conditioned medium was free of Murabutide. As expected, the “supernatant donor” monocytes stimulated with Murabutide preferentially differentiated into mo-DC compared to their control counterparts (Fig. 5B). Conditioned supernatant transferred after 3 and 6 hours to the “supernatant recipient” monocytes increased their differentiation into mo-DC (Fig. 5B). These results suggest that a soluble factor, secreted later than 1h after monocyte stimulation, promotes their differentiation into mo-DC.

IL-32 has been suggested to induce mo-DC differentiation (29). However, we were unable to measure any IL-32 secretion upon TLR ligand exposure, although other cytokines such as IL-6 were detected (Fig. S3C). We have previously shown that TNF- α promotes mo-DC differentiation in our culture model (22). Moreover, monocytes secreted high amounts of TNF- α after Murabutide exposure, starting after 1h and with a peak of secretion at 6h (Fig. 5C), consistent with the kinetics observed in the supernatant transfer experiment. We therefore evaluated further TNF- α as a candidate factor. We hypothesized that TNF- α and Murabutide have redundant effects in our model. To test this, we cultured monocytes with or without TNF- α in the cytokine cocktail (Fig. 5D). Murabutide and TNF- α induced mo-DC differentiation to the same extent, and the use of the two molecules combined resulted in an additive effect (Fig. 5D). To validate the role of TNF- α , we used neutralizing anti- TNF- α antibodies. The increased in mo-DC proportion due to Murabutide exposure was lower in the presence of anti- TNF- α antibodies compared to the isotype control (Fig. 5E). Of note, TNF- α secretion was not specific to NOD receptor stimulation, as TLR ligands also induced it (Fig. S3D). This suggests that the effect of TNF- α in monocytes can be counteracted by other signaling events induced upon TLR stimulation. Collectively, these results demonstrate that NOD receptor activation promotes mo-DC differentiation through the secretion of TNF- α .

TNF- α promotes mo-DC differentiation by inducing mi-R155

To address how TNF- α promotes mo-DC differentiation, we performed transcriptomic analysis on monocytes cultured for 3 and 6 hours with M-CSF and IL-4 in the presence or absence of TNF- α (Fig. 5F, Fig. S3E). As an internal control, we confirmed that monocytes exposed to TNF- α upregulated several genes of the TNF pathway at 3h (Fig. 5G). Moreover, monocytes exposed to TNF- α downregulated some genes of the mo-mac transcriptomic signature at 6h, consistent with an increased differentiation into mo-DC in response to TNF- α (Fig. 5G). Among the list of differentially expressed transcripts in TNF- α -exposed monocytes versus control monocytes, we selected miR-155 as a candidate (Fig. S3F), because miR-155 was previously shown in cell lines to target *MAFB* (30, 31). We validated by RT-qPCR that TNF- α induces miR-155 expression in monocytes with a peak at 3h and 6h (Fig. 5H). *MAFB* starts being expressed after 3h with a plateau at 6h and 12h (Fig. 4B), making the interaction with miR-155 possible in terms of kinetics. To address directly whether miR-155 targets *MAFB* in human monocytes, we measured its expression by RT-qPCR 6h after transfection of a miR-155 specific antagonist (antagomir) or a control sequence (scramble). MiR-155 antagomir increased the expression of *MAFB* in comparison to the control sequence, showing that miR-155 targets *MAFB* (Fig. 5I). Of note, Pam3 and Murabutide exposure (which induces high amounts of TNF- α) resulted in an increased expression of miR-155 (Fig. S3G). To test whether miR-155 promotes mo-DC differentiation, we cultured monocytes after transfection with the miR-155 antagomir or the control sequence. miR-155 antagomir decreased mo-DC and increased mo-mac differentiation, with or without Murabutide stimulation (Fig. 5J-K). In particular, in comparison to the control, miR-155 antagomir abrogated the increase in mo-DC differentiation induced by Murabutide. In conclusion, we found that miR-155 is necessary for monocyte differentiation into mo-DC in response to TNF- α exposure.

Pam3 and TNF- α promote the *in vivo* differentiation of mouse mo-mac and mo-DC respectively

To evaluate the *in vivo* relevance of our findings, we analyzed the differentiation of monocytes in mouse skin. We first addressed the impact of TLR signaling by analyzing skin cells 2 and 4 days following intradermal injections of Pam3. To select a panel of phenotypic markers allowing the identification of monocytes, mo-DC, mo-

mac and their differentiation intermediates, we refined a previously published flow cytometry strategy (32). We first performed unsupervised identification of CD45⁺lin⁻EpCam-Ly6G⁻ cells using FlowSOM (33). We found 11 cell clusters that we manually annotated based on the expression of nine myeloid cell markers (Fig. 6A, Fig. S4A). Consistent with the induction of inflammation, monocytes were increased in Pam3-treated mice at both timepoints (Fig. S4B). At day 4, we observed higher numbers of mo-mac in Pam3-treated mice compared to PBS-treated mice, while moDC were decreased at both timepoints (Fig. S4B). These results suggest that Pam3 exposure preferentially increases monocyte differentiation into mo-mac. To obtain a more quantitative evaluation of monocyte differentiation, we manually gated these populations (Fig. S4D). We focused on monocytes, differentiating monocytes, mo-mac, resident macrophages, mo-DC, neutrophils, Langerhans cells (LC), classical dendritic cell type 1 (DC1) and type 2 (DC2) (Fig. S4D). Two days after Pam3 injection, monocytes and neutrophils numbers were massively increased and remained high at day 4 (Fig. 6B, Fig. S4C). DC1 numbers were decreased following Pam3 injection at both times, while LC and DC2 were not changed (Fig. S4C). Upon Pam3 injection, we observed higher numbers of differentiating monocytes at both timepoints in comparison with PBS-treated mice, showing that the accumulated monocytes had started to differentiate (Fig. 6B). There were more mo-mac in the skin following Pam3 injection (Fig. 6B). Neither mo-DC nor resident macrophages were affected (Fig. 6B). However, Pam3 might increase both the differentiation and migration of mo-DC, resulting in apparent constant numbers in the skin. To address this hypothesis, we analyzed DC populations in the skin-draining lymph nodes (Fig. S4E). We could not detect in the lymph nodes any mo-DC population (expressing Ly6C or CD64), suggesting that mo-DC did not migrate upon Pam3-induced inflammation (Fig. S4E). By contrast, both resident and migratory DC2 numbers were increased (Fig. S4F). These observations are consistent with previous studies reporting poor migratory capacity for mo-DC (34–36). Collectively, these results show that Pam3 specifically increases mo-mac differentiation *in vivo*.

We then addressed the impact of TNF- α exposure. We employed the same strategy to analyse monocyte-derived cells two days following TNF- α injection. Based on the unsupervised FlowSOM analysis (Fig. S5A-B), we observed higher numbers of monocytes and mo-DC upon TNF- α injection (Fig. S5C). However, we did not

observe any change on the numbers of mo-mac (Fig. S5C). We further confirmed these observations by manually gating the different population (Fig. S5D). Monocyte and mo-DC numbers were increased while mo-mac counts were not changed, showing that monocytes preferentially differentiated into mo-DC (Fig. 6C). TNF- α exposure did not modify the other populations (Fig. 6C, Fig. S5E).

In conclusion, these results confirm that TLR activation increases mo-mac differentiation while TNF- α exposure promotes mo-DC in an *in vivo* setting.

Enrichment for mo-mac or mo-DC in human skin biopsies correlates with *in vivo* exposure to pathogens or TNF- α

Finally, we assessed the validity of our findings in an *in vivo* setting in humans. We analyzed the enrichment of monocyte, mo-mac and mo-DC transcriptomic signatures using Gene Set Enrichment Analysis (GSEA) (37) in relevant human samples using public microarray data sets. To determine the impact of TNF- α exposure on monocyte differentiation *in vivo*, we compared data sets of synovial samples from patients suffering from rheumatoid arthritis (RA) (an inflammatory disease in which TNF- α plays a major role in the pathogenesis) or osteoarthritis (OA) (a mechanical disorder that is considered independent of inflammation). Indeed, higher TNF- α level have been reported in synovial fluid of RA patients in comparison with OA patient (38). We used our previously published gene signatures for human mo-DC (and mo-mac), defined as the genes enriched in ascites mo-DC (or mo-mac) compared to ascites mo-mac (or mo-DC) and blood CD14⁺ monocytes (22). The monocyte signature was enriched in RA versus OA samples in some data sets, consistent with the known recruitment of monocytes in the inflamed joints in RA (39) (Fig. 6D). The mo-DC signature was significantly enriched in RA versus OA samples in all data sets analyzed (Fig. 6D and Fig. S6A). Of note, the mo-mac signature was only enriched in OA versus RA samples in some data sets. Consistent with its induction by TNF- α , miR-155 was expressed at higher levels in RA compared to OA synovial tissue (Fig. S6B). Overall, these results are consistent with our finding that TNF- α promotes mo-DC differentiation.

To assess the impact of pathogen recognition, we analyzed skin biopsies from volunteers experimentally infected with Herpes Simplex Virus type 2 (HSV2) and compared infected skin with healthy skin from the same individuals, during infection

or after resolution (40). We found that the monocyte and mo-mac signatures were enriched in HSV2-infected skin compared to healthy skin, while none of the 3 signatures was enriched in healed skin compared to healthy skin (Fig. 6E and Fig. S6C). These results support our findings that viruses increase mo-mac differentiation.

Discussion

In this study, we have demonstrated that pathogen recognition skews monocyte differentiation into macrophages versus DC. We showed that viruses strongly promote mo-mac differentiation and inhibit mo-DC development. By contrast, mycobacteria favor mo-DC development. We evidenced that TLR activation redirects monocyte differentiation towards mo-mac by inhibiting IRF4 and inducing MAFB expression. On the other hand, NOD receptor activation promotes mo-DC differentiation through autocrine TNF- α and miR-155 expression.

During infections, monocytes encounter pathogens containing various pathogen-associated molecular patterns (PAMPs) that can potentially trigger many different signaling pathways. In the face of such complex stimulation, cells make signaling decisions to either integrate multiple signals, resulting in synergy or antagonism, or activate signaling pathways independently without any cross-talk (41, 42). We found that Mycobacteria, which contain both TLR and NOD ligands, increase mo-DC differentiation. This suggests that, during Mycobacteria recognition, TLR signaling is counteracted by NOD activation in monocytes. This is consistent with previous studies showing that NOD receptors negatively regulate TLR-induced NF- κ B signaling in mouse bone marrow-derived macrophages and splenic myeloid cells (24, 25). Simplification of signaling integration has also been suggested in DC exposed to triple PAMPs stimulations, where the sensing outcome was similar to that of single compounds or pairs (43). Our observation that TLR activation favors mo-mac differentiation despite high secretion of TNF- α suggests that signaling prioritization may also extend to the simultaneous activation of separate NF- κ B -dependent pathways, such as TLR and TNF-receptor signaling. Finally, pathogens may activate other receptors such as RIG-I like, AIM2-like and C-type lectin receptors. The impact

of these signaling pathways on monocyte differentiation remains open for future investigation.

In the past few years, numerous studies have described the ability of innate immune cells to acquire a memory response following PAMP sensing, which has been termed 'trained immunity'. This phenomenon has first been demonstrated in the context of monocyte to macrophage differentiation. Indeed, macrophages differentiated from β -glucan-exposed monocytes secreted higher levels of pro-inflammatory cytokines following stimulation with various PAMPs or whole pathogen (44, 45). By contrast, macrophages exposed to LPS secreted lower levels of pro-inflammatory cytokines following a second stimulation with LPS (46), which is referred to as 'LPS tolerance'. For both trained immunity and tolerance, only mo-mac have been studied and whether the same phenomenon occurs in mo-DC has remained unclear. Here, we show that mo-mac and mo-DC differentiated from Pam3- and Murabutide-exposed monocytes secreted decreased levels of pro-inflammatory cytokines after stimulation with various PAMPs. Our results show that, similar to mo-mac, mo-DC can be imprinted for tolerance. LPS tolerance has been associated with enhanced phagocytic capacities and reduced antigen presentation abilities in macrophages derived from monocytes (47). However, we found that mo-DC differentiated from Pam3- and Murabutide-exposed monocytes were more efficient for stimulating T cell proliferation. Moreover, mo-DC and mo-mac differentiated from monocytes activated with Pam3 and Murabutide displayed decreased phagocytic capacities.

Recent studies have demonstrated a role for mTOR during myelopoiesis. The deletion of mTOR or of the mTORC1 component Raptor in mice strongly reduces the development of monocytes and neutrophils (48–50). Here, we evidenced a role for mTORC1 in the differentiation of monocytes into mo-mac. We found that mTORC1 activation induces MAFB expression, which is essential for mo-mac differentiation (22). This is in contrast with the upregulation of MAFB detected in granulocyte-monocyte progenitors from mTOR KO mice (50). However, osteoclast treatment with rapamycin increased MAFB showing that mTOR inhibits MAFB expression in these cells (51). This suggests that the effect of mTOR on MAFB expression may be cell-specific.

It has been demonstrated that following TLR stimulation with LPS, poly-IC or CpG, bone marrow-derived macrophages (52) and human mo-DC (53) upregulate miR-155 expression. Here we show that TNF- α exposure induces the expression of miR-155 in human monocytes. This suggests that increased miR-155 expression following TLR activation is mediated by TNF- α . miR-155 has pleiotropic effects in immune cells. It is involved in granulocyte/monocyte proliferation in mouse bone marrow (54), polarization of bone marrow-derived macrophages toward a pro-inflammatory state (55) and maturation of bone marrow-derived DC (56). Here we demonstrate that in addition to its role in the proliferation and function of myeloid cells, miR-155 is also essential for monocyte differentiation towards mo-DC. We further show that *MAFB* is a target of miR-155 in human monocytes. We have previously observed that *MAFB* silencing in monocytes favors mo-DC differentiation (22). Thus, increased mo-DC differentiation in response to TNF- α could be due to *MAFB* targeting by miR-155. However, we cannot exclude that other targets of miR-155 could be involved in this process. Finally, miR-155 expression has been associated with RA severity. Synovial fluid monocytes and synovial tissue macrophages from RA patients express higher levels of miR-155 than that of OA patients (55, 57). This is consistent with the induction of miR-155 expression by TNF- α , which is highly secreted in inflamed RA joints. In monocytes from RA patients and healthy donors, miR-155 expression also induces pro-inflammatory cytokine secretion including TNF- α (55, 58). This suggests the existence of an amplification loop between TNF- α and miR-155 potentially exacerbating the immunopathology.

Manipulating the differentiation of monocytes into mo-DC versus mo-mac represents an appealing strategy to dampen inflammation or promote immune responses, depending on the context. This strategy is hindered by a limited knowledge of the mechanisms driving monocyte fate decision and differentiation. Here we identified mTORC1 and mir-155 as modulators of this process. By providing a better understanding of the molecular regulation of monocyte differentiation, these results should open up possibilities for therapeutic opportunities.

Author Contributions

Conceptualization: ACo and ES. Methodology: ACo, LG, ES. Formal analysis: ACo, LG, ES. Investigation: ACo, AdJ, ACr, ES. Writing – original draft: ACo and ES. Writing – review and editing: all authors. Visualization: ACo and ES. Supervision: ES. Funding acquisition: ES.

Acknowledgements

This work was funded by INSERM, Institut Curie (CIC IGR-Curie 1428) and Agence Nationale de la Recherche (ANR-10-LABX-0043, ANR-10-IDEX-0001-02 PSL and ANR-17-CE15-0011-01). ACo is a fellow of Fondation pour la Recherche Médicale (FDT202001010805). The authors wish to thank the Flow Cytometry Platform of Institut Curie, the Next Generation Sequencing Platform of Institut Curie and the In vivo Experiments Platform of Institut Curie, B. Manoury and M. Burbage for critical reading of the manuscript and Javiera Villar for technical assistance.

Competing interests

The authors declare no competing interests.

Material and methods

Human blood, monocyte isolation and culture

Buffy coats from healthy donors were obtained from Etablissement du Sang Francais (EFS) in accordance with INSERM ethical guidelines. According to French Public Health Law (art L 1121–1-1, art L 1121–1-2), written consent and Institutional Review Board approval are not required for human noninterventional studies. Peripheral blood mononuclear cells were obtained by centrifugation on a ficoll gradient (Lymphoprep, StemCell). Blood monocytes were then positively isolated using CD14⁺ microbeads (Miltenyi) according to the manufacturer's recommendations. Monocytes ($2 \cdot 10^6$ /mL) were cultured for 5 days with RPMI-Glutamax (Gibco) supplemented with antibiotics (penicillin and streptomycin) and 10% fetal calf serum (FCS) in the presence of 100ng/mL M-CSF (Miltenyi), 5ng/mL IL-4 (Miltenyi) and 5ng/mL TNF- α (Miltenyi). Where indicated, 1ug/mL Pam3 (Invivogen), 1,25 ug/mL LPS (Invivogen), 2ug/mL Gardiquimod (Invivogen), 100ng/mL R848 (Invivogen), 10ug/mL Murabutide (Invivogen), 10ug/mL TriDAP (Invivogen), 20 ug/mL formalin inactivated Influenza A (Charles River), sendai virus (Charles River), heat killed *Mycobacterium butyricum* (Fisher Scientific), were added at the beginning of the culture and were extensively washed after 30 minutes or not washed. For the inhibition of mTORC1 signaling, monocytes were cultured with 25nM temsirolimus (Sigma). For the neutralization of TNF- α , monocytes were cultured in the presence of 2ug/mL anti-TNF- α neutralizing ab (R&D Biotechne) or mouse IgG1 isotype control (R&D Biotechne). For the inhibition of miR-155, monocytes were transfected with TransIT-X2 (Mirus) and 5 pmol miR-155 antagomir (Thermo Fisher Scientific) or control sequence (Thermo Fisher Scientific) and cultured with the cytokines and Murabutide as previously described for 5 days. For the inhibition of RIPK2 signaling, monocytes were pre-incubated with 1 μ M GSK583 (R&D Biotechne) for 30 minutes, and Murabutide or heat killed *Mycobacterium tuberculosis* (Invivogen) was added.

Flow cytometry of monocyte-derived cells

After 5 days of culture, cells were detached using cold PBS containing 0,5% human serum and 2mM EDTA. Staining details can be found in Supplementary Information. Cells were acquired on a FacsVerse instrument (BD Biosciences). In the monocyte

differentiation assay, we set for each individual donor the CD1a+ and CD16+ gates on the medium condition and then apply these gates to the different test conditions. To quantify the expression of activation markers, the Stain Index was calculated as follows: $(MFI_{\text{sample}} - MFI_{\text{isotype}}) / (SD_{\text{isotype}})$. MFI represents the Median of fluorescence and SD the standard deviation.

Cytokine secretion

Culture details can be found in Supplementary Information. Secretion of IL-8, IL-6 and TNF- α was measured by cytometric bead array (BD Biosciences).

Reverse transcription quantitative PCR

Details on sample preparation can be found in Supplementary Information. The second derivative method was used to determine each Cp and the expression of genes of interest relative to the housekeeping genes.

Western blot

Details on membrane preparation can be found in Supplementary Information. Primary antibodies were against IRF4 (Cell signaling), MAFB (NovusBio), gp96 (clone 9G10, Enzo Life Sciences) and actin (Millipore, clone C4). Images were acquired using a chemidoc instrument (Bio-rad) and quantified with Fiji software.

Morphological analysis of mo-mac and mo-DC

Cells were placed on slides using a cytospin centrifuge and were stained with May-Grünwald (Sigma) and Giemsa (Merck) solutions. Pictures were acquired using a Leica DM 4000 B microscope with a ProgRes SpeedXTcore 5 camera.

CD4 T cell proliferation and polarization

Naive or memory CD4 T cells were isolated from PBMCs using negative isolation kits (Stemcell) according to the manufacturer's recommendations. Following 5 days of culture, mo-mac and mo-DC were sorted on a facs Aria instrument (BD Biosciences) after staining with anti-CD16 FITC and anti-CD1a APC. To assess T cell proliferation, T cells were stained with CellTrace Violet (Thermo Fisher Scientific). 1.250, 2.500, 5.000, 10.000 APC were cultured with 50.000 allogenic naive or memory T cells in Yssel Medium supplemented with 10% FCS. After 6 days, T cells were stained with

fixable viability efluor 780 dye (Thermo Fisher Scientific) for 10 minutes at 4°C and counted using counting beads on a facs verse instrument.

To assess Th cell polarization, 20.000 APC were cultured with 50.000 allogenic naive T cells in Yssel Medium supplemented with 10% FCS. After 6 days, T cells were washed and stimulated in X-Vivo TM 15 (Lonza) without FCS in the presence of PMA (50 ng/ml), ionomycin (1 µg/ml), and BFA (4 µg/ml; Sigma-Aldrich) for 5 hours at 37°C. Cells were then washed, stained with fixable viability efluor 780 dye, fixed and permeabilized (Intracellular Fixation and Permeabilization Buffer Set, ebioscience). The cells were then stained for intracellular cytokines in a buffer containing 2% mouse serum (Thermo fisher Scientific) and human Fcblock (BD Biosciences) for 1 hour at room temperature with the following antibodies: anti-IL-4 APC (ebiosciences, 8D4-8), anti-IL21 PE (BD Biosciences, clone 3A3-N2.1), anti-IFNγ PeCy7 (ebiosciences, clone 4S.B3). Samples were acquired on a facs verse instrument.

Phagocytosis

Monocytes were cultured in RPMI (Gibco) supplemented with 10% FCS and antibiotics in the presence of M-CSF, IL-4, TNF-α and 1ug/mL Pam3 or 10ug/mL Murabutide. After 5 days, cells were detached and plated in 96-well plates. After 30 minutes, pHrodo green S.Aureus (Fischer Scientific) were added to the cells. Cells were washed with cold PBS, and stained with fixable zombie NIR (Biolegend) for 10 min at 4°C. Cells were then stained with TruStain blocking solution, anti-CD16 FITC and anti-CD1a APC and fixed with 4% PFA for 10 minutes at 4°C. The samples were acquired on a facs verse instrument.

Gene Set Enrichment Analysis

GSEA was performed using the GSEA software (version 4.0.3) with the default parameters, except for the number of permutations that we fixed at n=1000. Datasets were downloaded from GEO (GSE18527, GSE55235, GSE1919, GSE12021, GSE55584, GSE55457, GSE89408). Count matrix from RNA-seq studies were first normalized using DESeq2. Gene signatures of blood monocytes, mo-DC and mo-mac were designed from microarray data (22).

RNA-seq analysis

Monocytes were culture in RPMI supplemented with 10% FCS in the presence of MSCF, IL-4 and in the presence or absence of TNF- α . Monocytes cultured for 3 and 6 hours were lyzed in RLT buffer (Qiagen). Details on library preparation can be found in Supplementary Information. Differential gene expression analysis was performed using *DESeq2* (59). Details on the analysis pipeline can be found in Supplementary Information. Data are accessible through GEO Series accession number GSE166043.

Analysis of mouse skin and lymph nodes

50 μ g Pam3, 150ng TNF- α or PBS as control were injected intradermally in both ears of C57B6/J mice. Ears were harvested and analyzed as previously described (60). Briefly, the two layers of each ear were separated and incubated overnight at 4°C in 0.2mg/mL dispase II (Roche). Ears were then cutted in small pieces and incubated 90 minutes at 37°C in digestion mix containing 0.5mg/mL DNase I (Sigma) and 1.5mg/mL collagenase IV (Worthington Biochemical Corporation). Ear-draining lymph nodes were harvested, cut in small pieces and incubated for 30 minutes at 37°C with 2mg/mL Collagenase D (Roche) and 0.1mg/mL DNase I (Roche). Cell suspensions were filtered using 40 μ M cell strainers. Staining details can be found in Supplementary Information. Cells were acquired on a spectral flow cytometer (Aurora instrument, Cytex). Details on data analysis can be found in Supplementary Information.

Software and stastistical analysis

Flow cytometry data were analysed using FlowJo software v10 (Tree Star). Statistical analyses were performed using Prism software v7 (GraphPad). For all analyses, paired Wilcoxon tests were used.

Figure legends

Figure 1. Pathogen recognition impacts monocyte differentiation

Monocytes were cultured for 5 days with M-CSF, IL-4 and TNF- α . Monocyte-derived cells were stained for CD16 and CD1a and analyzed by flow cytometry. (A) CD16+ mo-mac, CD1a+ mo-DC and CD16-CD1a- undifferentiated cells were sorted and stained with May Grunwald – Giemsa solutions after cytopspin. Bar = 30 μ M.

Representative images (n=5). (B-D) Proportions of mo-mac and mo-DC at day 5 after monocyte exposure to inactivated Influenza A virus (Flu, B, n=12), live Sendai Virus (C, n=8), heat-killed *Mycobacterium butyricum* (MB, D, n=15). Each symbol represents one individual donor. (E) Monocytes were pre-incubated with GSK583, heat-killed *Mycobacterium tuberculosis* (MT) was added and differentiation was analyzed after 5 days of culture. Wilcoxon test. *, P<0.05; **, P<0.01; ***, P<0.001; ****, P<0.0001.

Figure 2. TLR ligands promote mo-mac while NOD ligands induce mo-DC differentiation

Monocytes were cultured for 5 days with M-CSF, IL-4 and TNF- α with indicated ligands. Monocyte-derived cells were stained for CD16 and CD1a and analyzed by flow cytometry. (A-G) Representative results. (B-F) Proportions of mo-mac and mo-DC at day 5 after monocyte exposure to Pam3 (B, n=39), Gardiquimod (Gardi, C, n=29), LPS (D, n=28), Murabutide (Mura, E, n=41), TriDAP (F, n=21). Each symbol represents one individual donor. (G) Expression of the surface markers CD163, MERTK, CD88, CD206, CD226 and CD1b was analyzed on mo-mac and mo-DC at day 5 after monocyte exposure to Pam3 or Murabutide. Empty histograms correspond to isotype controls. Representative of 4 independent experiments. *, P<0.05; **, P<0.01; ***, P<0.001; ****, P<0.0001.

Figure 3. Monocyte exposure to TLR or NOD receptor ligands modifies the functional properties of mo-mac and mo-DC

Monocytes were cultured for 5 days with M-CSF, IL-4 and TNF- α in the presence or absence of Pam3 or Murabutide (Mura). At day 5, mo-mac and mo-DC were sorted, and assessed for cytokine secretion, ability to induce T cell proliferation and polarization, and phagocytic properties. (A) Scheme of the experimental setup. (B) Sorted mo-DC and mo-mac were stimulated for 24 hours with Pam3, LPS, R848, or Murabutide. TNF- α , IL-6 and IL-8 secretion was measured in supernatants. For mo-DC, n>8 and for mo-mac, n>9. (C-D) Sorted mo-DC and mo-mac were co-cultured with blood allogenic naïve CD4 T cells for 6 days. (C) Proliferation of CD4 T cells was analyzed by measuring the dilution of a proliferation trace dye (CTV). Representative histograms and percentage of CTV- cells are shown. For mo-DC, n>10 and for mo-

mac, n>9. (B,C) The median and interquartile range are represented. (D) Polarization of CD4 T cells was assessed by intracellular flow cytometry after staining for IFN γ , IL-4 and IL-17. (n>9). (E) Monocyte-derived cells were incubated with pHrodo *S.aureus* bioparticles conjugates for 10, 20 or 30 minutes at 37°C. Phagocytosis was assessed by measuring the fluorescence emitted by phagocytosed bacteria, and defined using the negative control (incubation at 4°C). (n=9). Wilcoxon test. *, P<0.05; **, P<0.01. Each symbol represents an individual donor.

Figure 4. **TLR ligands modify the balance of IRF4 and MAFB expression through mTORC1 activation**

Monocytes were cultured with M-CSF, IL-4 and TNF- α in the presence or absence of indicated TLR ligands. (A,B,C,E) mRNA expression of IRF4 (A,C) and MAFB (B,E) were measured by RT-qPCR at indicated timepoints. (D,F) Protein expression of IRF4 (D) and MAFB (F) were measured by Western blot at indicated timepoints. Relative protein expression was assessed by densitometry as compared to actin or GP96. (n>6). (G,H) Monocytes were cultured for 2 hours in the presence or absence of Pam3, Gardiquimod (Gardi) and temsirolimus (temsi). (G) Protein expression of phospho-rpS6 or actin was measured by Western blot. Representative of 6 donors. (H) Relative protein expression was assessed by densitometry as compared to actin. (n=6). (I,J) IRF4 (I) and MAFB (J) expression were measured by RTqPCR after 3h and 12h of culture respectively. Percentage of change of IRF4 and MAFB expression in the Pam3 condition versus the control condition in the presence or absence of temsirolimus were calculated. (n=9). Each symbol represents an individual donor. Wilcoxon test. *, P<0.05; **, P<0.01; ***, P<0.001; ****, P<0.0001.

Figure 5. **NOD receptor ligands promote mo-DC differentiation through TNF- α secretion and miR-155 expression**

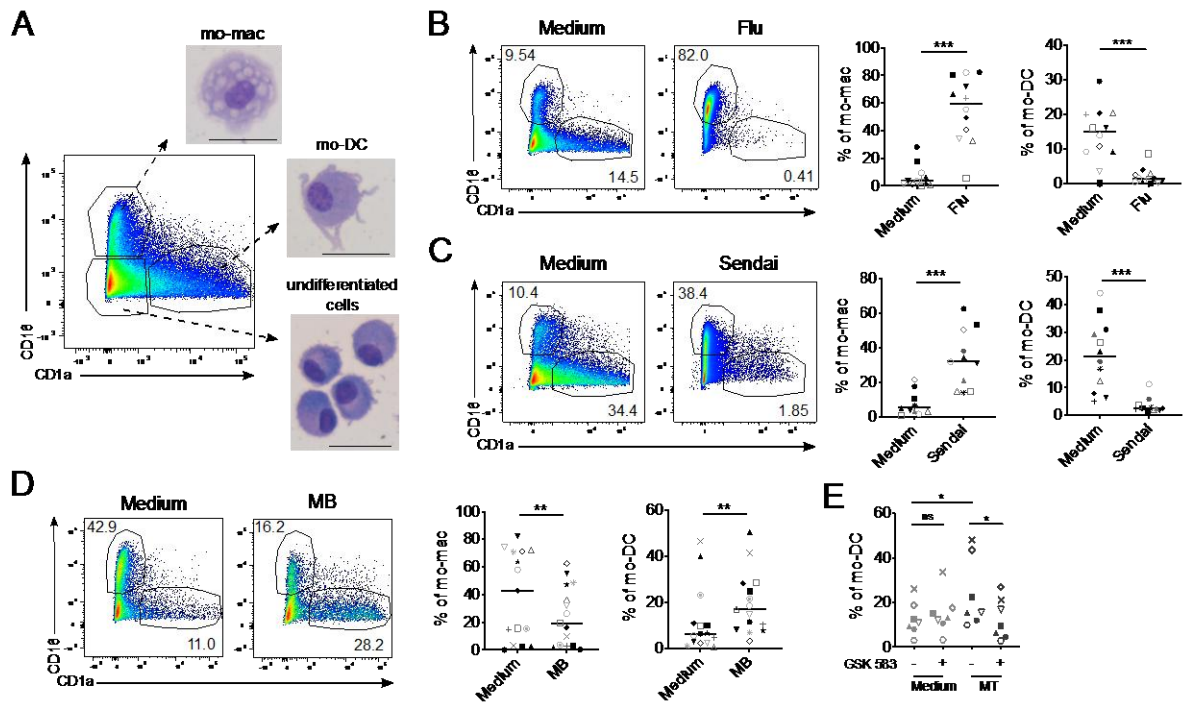
(A) Experimental setup for the supernatant transfer experiment. (B) Mo-DC percentages after 5 days in “supernatant donor” and “supernatant recipient” cultures. (n=11). (C) Monocytes were cultured with M-CSF and IL-4 in the presence or absence of Murabutide (Mura). After 1, 3, 6 and 24 hours, TNF- α secretion in supernatants was measured (n>9). (D) Monocytes were cultured for 5 days with M-CSF and IL-4 in the presence or absence of Murabutide or TNF- α (n=12). (E)

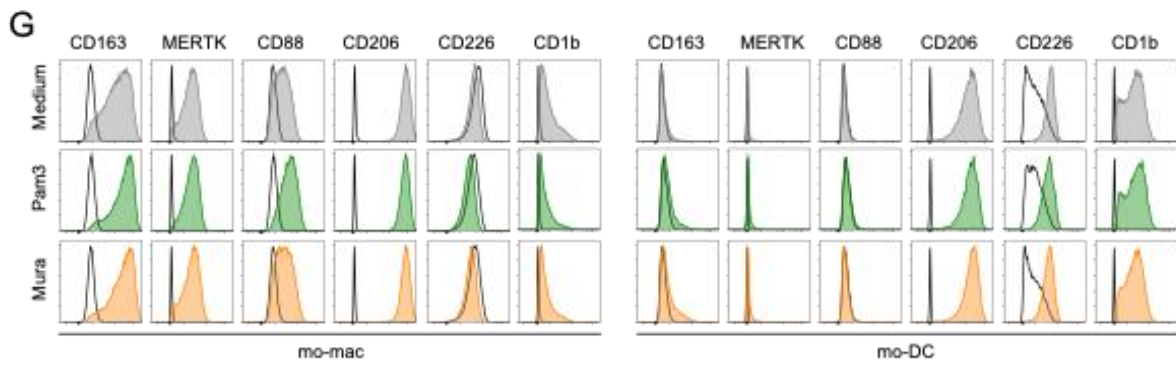
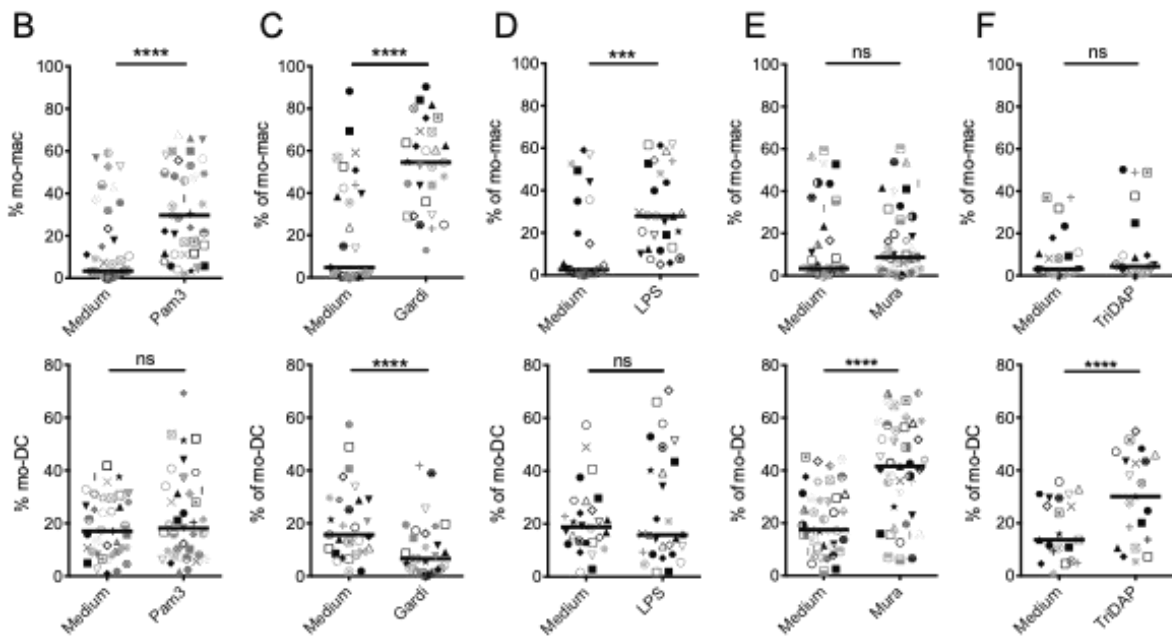
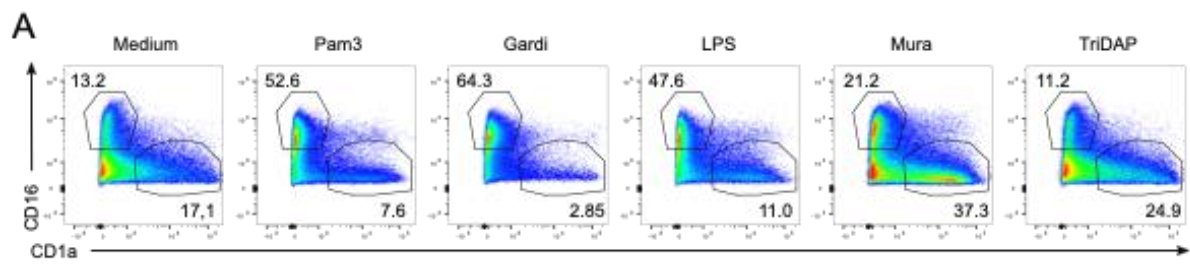
Monocytes were cultured for 5 days with M-CSF and IL-4 in the presence or absence of Murabutide, anti-TNF- α neutralizing antibodies or isotype control antibodies (n=17). Proportions of mo-DC (left) and percentage of change in mo-DC proportion in the Murabutide condition versus the control condition with the anti-TNF- α antibody or isotype control (right) (n=17). (F-G) Monocytes were cultured with M-CSF and IL-4 in the presence or absence of TNF- α for 3 and 6 hours and analyzed by RNA-sequencing (n=5). (F) Differentially expressed genes in the presence of TNF- α versus control condition at 3h. (G) Scaled expression of genes from the TNF pathway and from the mo-mac signature in each sample at indicated timepoints. Each column represents an individual donor. D=donor. student t test, *P<0.05, **P<0.01, ***P<0.001 (H) Monocytes were cultured with M-CSF, IL-4 in the presence or absence of TNF- α . At different timepoints, miR-155 expression was measured by RTqPCR. (I-K) Monocytes were transfected with a miR-155 antagonist (antagomir) or a control sequence and cultured with M-CSF, IL-4 and TNF- α . (I) *MAFB* expression was determined by RT-qPCR after 6 hours. (n=9). (J-K) Monocytes differentiation after 5 days of culture. (J) Representative results (n=9) (K) Proportions of mo-DC and mo-mac. (n=9). Wilcoxon test. *, P<0.05; **, P<0.01; ***, P<0.001; ****, P<0.0001. Each symbol represents one donor.

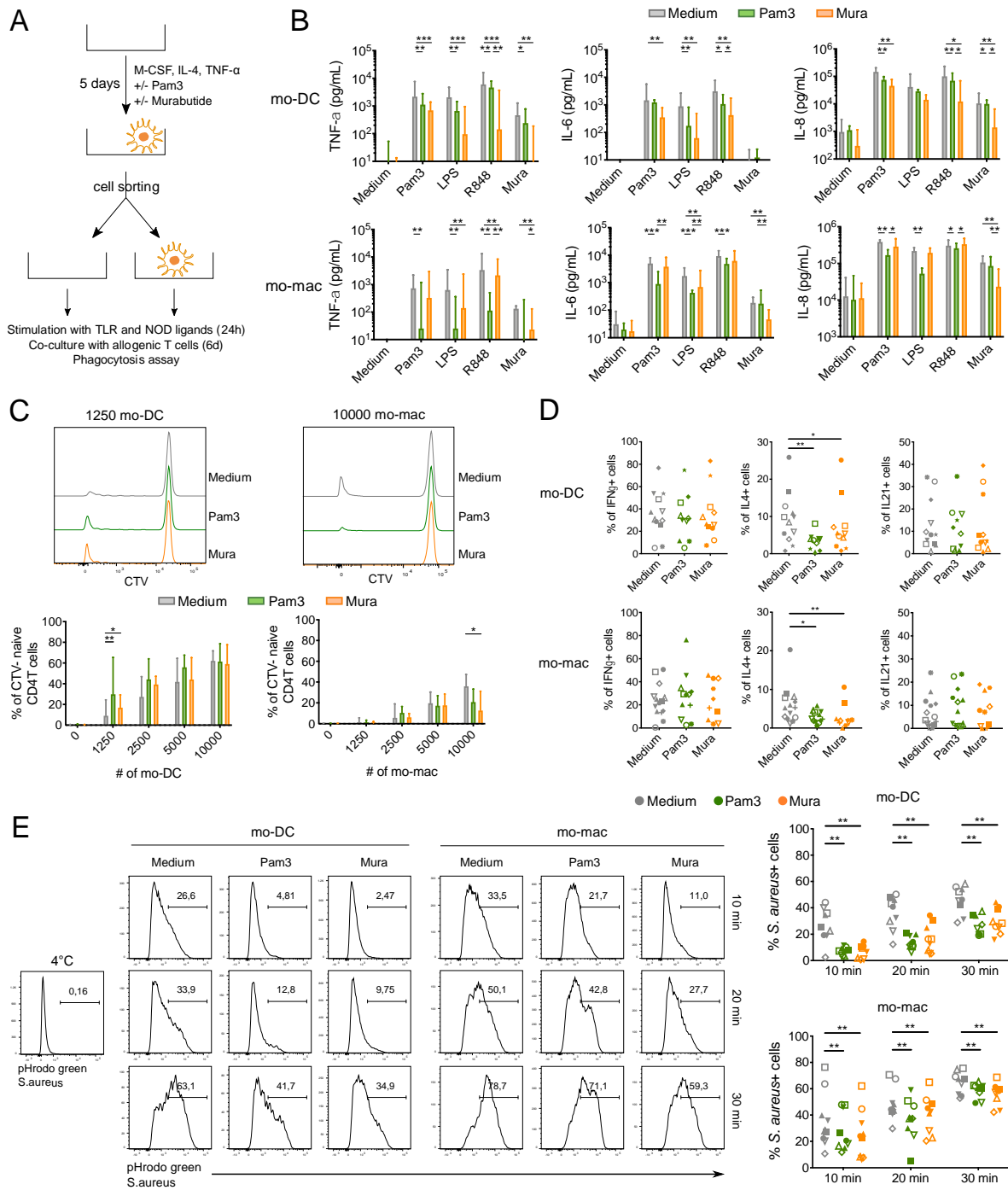
Figure 6. *In vivo* exposure to TLR ligands or TNF- α correlates with increased mo-mac or mo-DC differentiation

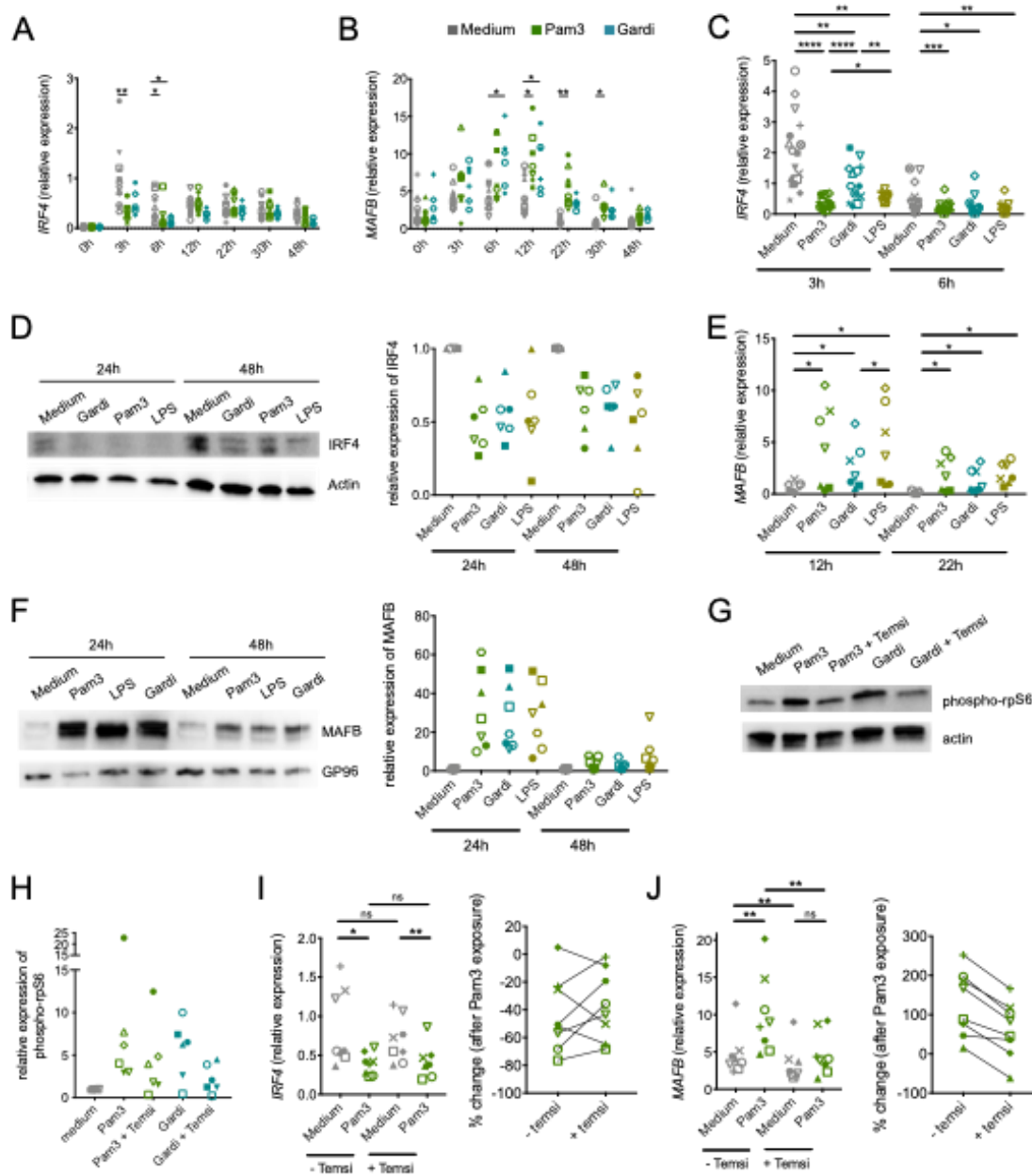
(A-C) Pam3, TNF- α or PBS as control, was injected intradermally in ears of C57B6/J mice. Single cell suspensions were prepared by mechanical and enzymatic digestion. (A) UMAP representation of the 11 cell clusters identified by FlowSOM unsupervised analysis. Each dot represents an individual cell. N=5 mice in 2 independent experiments. (B-C) Total cell numbers of monocytes, differentiating monocytes, mo-mac, resident macrophages (resident mac) and mo-DC are represented upon Pam3 (B, day 2 (D2) and day 4 (D4)) or TNF- α (C, day 2) injection. Each symbol corresponds to an individual mouse (3 independent experiments). Student T test. *, P<0.05; **, P<0.01; ***, P<0.001; ****, P<0.0001. (D-E) Gene expression data was extracted from indicated public datasets. Gene set enrichment analysis (GSEA) was performed for monocyte, mo-DC and mo-mac gene signatures. BubbleGUM representations of the GSEA results are shown. (D) GSEA on datasets from synovial

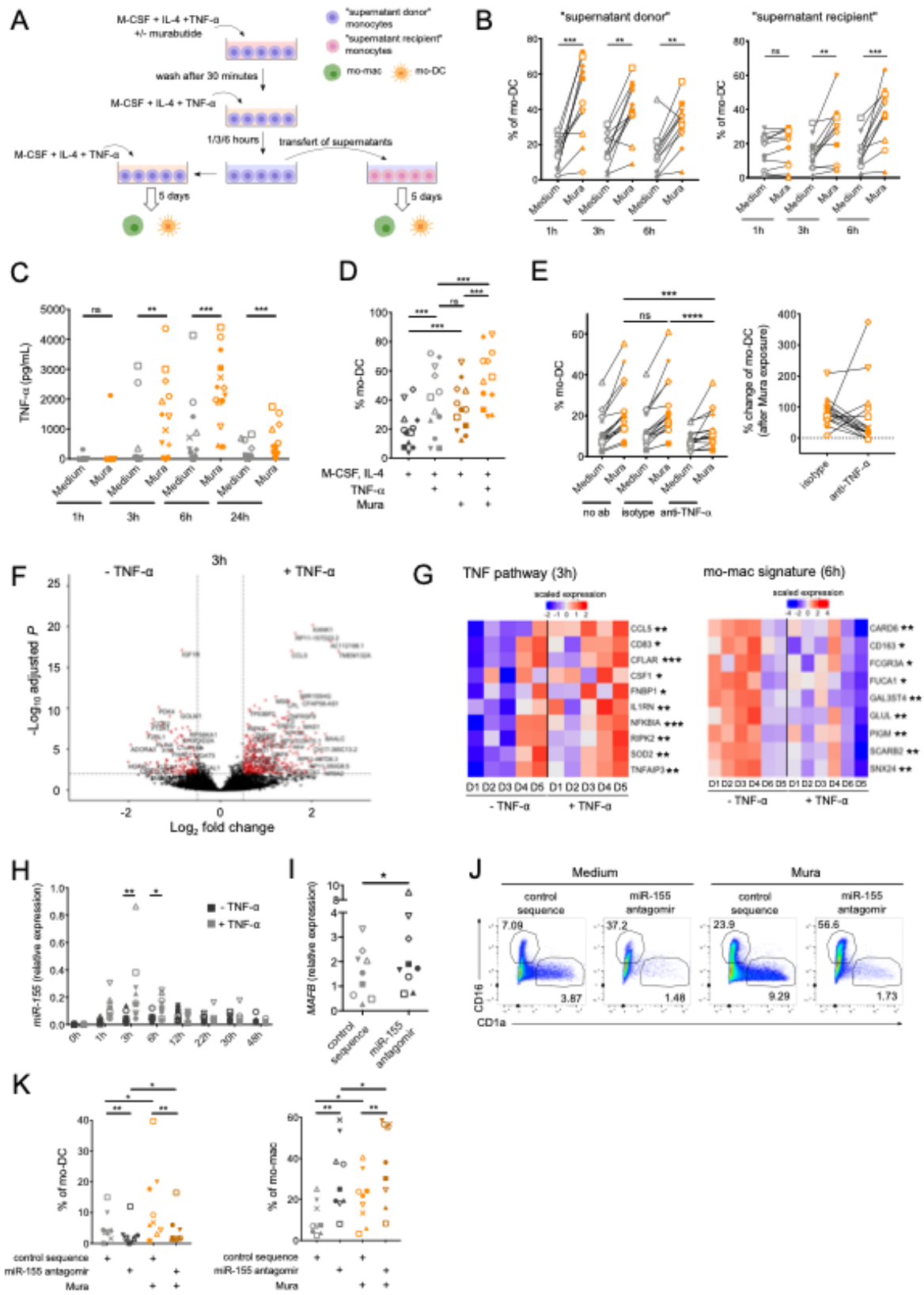
biopsies from joints of rheumatoid arthritis (RA) or osteoarthritis (OA) patients. (E) GSEA on datasets from skin biopsies from lesional or healthy skin of Herpes simplex virus 2 (HSV2) infected patients. The normalized enrichment score (NES) and the false discovery rate (FDR) correspond to the strength and the significance of the result respectively. ns= not significant











Bibliography

1. Davies LC, Jenkins SJ, Allen JE, Taylor PR (2013) Tissue-resident macrophages. *Nat Immunol* 14(10):986–995.
2. Shi C, Pamer EG (2011) Monocyte recruitment during infection and inflammation. *Nat Rev Immunol* 11(11):762–774.
3. Serbina NV, Pamer EG (2006) Monocyte emigration from bone marrow during bacterial infection requires signals mediated by chemokine receptor CCR2. *Nat Immunol* 7(3):311–317.
4. Tsou C-L, et al. (2007) Critical roles for CCR2 and MCP-3 in monocyte mobilization from bone marrow and recruitment to inflammatory sites. *J Clin Invest* 117(4):902–909.
5. Shi C, et al. (2010) Monocyte trafficking to hepatic sites of bacterial infection is chemokine independent and directed by focal intercellular adhesion molecule-1 expression. *J Immunol* 184(11):6266–6274.
6. Lim JK, et al. (2011) Chemokine receptor Ccr2 is critical for monocyte accumulation and survival in West Nile virus encephalitis. *J Immunol* 186(1):471–478.
7. Peters W, et al. (2001) Chemokine receptor 2 serves an early and essential role in resistance to Mycobacterium tuberculosis. *Proc Natl Acad Sci USA* 98(14):7958–7963.
8. Haist KC, Burrack KS, Davenport BJ, Morrison TE (2017) Inflammatory monocytes mediate control of acute alphavirus infection in mice. *PLoS Pathog* 13(12):e1006748.
9. Jakubzick CV, Randolph GJ, Henson PM (2017) Monocyte differentiation and antigen-presenting functions. *Nat Rev Immunol* 17(6):349–362.
10. Williams M, Mildner A, Yona S (2018) Developmental and functional heterogeneity of monocytes. *Immunity* 49(4):595–613.
11. Blériot C, et al. (2015) Liver-resident macrophage necroptosis orchestrates type 1 microbicidal inflammation and type-2-mediated tissue repair during bacterial infection. *Immunity* 42(1):145–158.
12. Machiels B, et al. (2017) A gammaherpesvirus provides protection against allergic asthma by inducing the replacement of resident alveolar macrophages with regulatory monocytes. *Nat Immunol* 18(12):1310–1320.
13. Aegerter H, et al. (2020) Influenza-induced monocyte-derived alveolar macrophages confer prolonged antibacterial protection. *Nat Immunol* 21(2):145–157.
14. Williams M, Svedberg FR (2021) Does tissue imprinting restrict macrophage plasticity? *Nat Immunol* 22(2):118–127.
15. Wakim LM, Waithman J, van Rooijen N, Heath WR, Carbone FR (2008) Dendritic cell-induced memory T cell activation in nonlymphoid tissues. *Science* 319(5860):198–202.
16. Ma Y, et al. (2013) Anticancer chemotherapy-induced intratumoral recruitment and differentiation of antigen-presenting cells. *Immunity* 38(4):729–741.
17. Honda T, et al. (2014) Tuning of antigen sensitivity by T cell receptor-dependent negative feedback controls T cell effector function in inflamed tissues. *Immunity* 40(2):235–247.
18. Aldridge JR, et al. (2009) TNF/iNOS-producing dendritic cells are the necessary evil of lethal influenza virus infection. *Proc Natl Acad Sci USA* 106(13):5306–5311.
19. Ellis GT, et al. (2015) TRAIL+ monocytes and monocyte-related cells cause

- lung damage and thereby increase susceptibility to influenza-Streptococcus pneumoniae coinfection. *EMBO Rep* 16(9):1203–1218.
20. Williams M, et al. (2009) IL-10 dampens TNF/inducible nitric oxide synthase-producing dendritic cell-mediated pathogenicity during parasitic infection. *J Immunol* 182(2):1107–1118.
 21. Greter M, et al. (2012) GM-CSF controls nonlymphoid tissue dendritic cell homeostasis but is dispensable for the differentiation of inflammatory dendritic cells. *Immunity* 36(6):1031–1046.
 22. Goudot C, et al. (2017) Aryl Hydrocarbon Receptor Controls Monocyte Differentiation into Dendritic Cells versus Macrophages. *Immunity* 47(3):582–596.e6.
 23. Desalegn G, Pabst O (2019) Inflammation triggers immediate rather than progressive changes in monocyte differentiation in the small intestine. *Nat Commun* 10(1):3229.
 24. Watanabe T, Kitani A, Murray PJ, Strober W (2004) NOD2 is a negative regulator of Toll-like receptor 2-mediated T helper type 1 responses. *Nat Immunol* 5(8):800–808.
 25. Udden SMN, et al. (2017) NOD2 suppresses colorectal tumorigenesis via downregulation of the TLR pathways. *Cell Rep* 19(13):2756–2770.
 26. Weichhart T, et al. (2008) The TSC-mTOR signaling pathway regulates the innate inflammatory response. *Immunity* 29(4):565–577.
 27. Schmitz F, et al. (2008) Mammalian target of rapamycin (mTOR) orchestrates the defense program of innate immune cells. *Eur J Immunol* 38(11):2981–2992.
 28. Erra Díaz F, et al. (2020) Extracellular Acidosis and mTOR Inhibition Drive the Differentiation of Human Monocyte-Derived Dendritic Cells. *Cell Rep* 31(5):107613.
 29. Schenk M, et al. (2012) NOD2 triggers an interleukin-32-dependent human dendritic cell program in leprosy. *Nat Med* 18(4):555–563.
 30. Yang L, Li R, Xiang S, Xiao W (2016) MafB, a target of microRNA-155, regulates dendritic cell maturation. *Open Life Sci* 11(1).
 31. Kim H (2017) The transcription factor MafB promotes anti-inflammatory M2 polarization and cholesterol efflux in macrophages. *Sci Rep* 7(1):7591.
 32. Tamoutounour S, et al. (2013) Origins and functional specialization of macrophages and of conventional and monocyte-derived dendritic cells in mouse skin. *Immunity* 39(5):925–938.
 33. Van Gassen S, et al. (2015) FlowSOM: Using self-organizing maps for visualization and interpretation of cytometry data. *Cytometry A* 87(7):636–645.
 34. Bosteels C, et al. (2020) Inflammatory Type 2 cDCs Acquire Features of cDC1s and Macrophages to Orchestrate Immunity to Respiratory Virus Infection. *Immunity* 52(6):1039–1056.e9.
 35. Nakano H, et al. (2009) Blood-derived inflammatory dendritic cells in lymph nodes stimulate acute T helper type 1 immune responses. *Nat Immunol* 10(4):394–402.
 36. Langlet C, et al. (2012) CD64 expression distinguishes monocyte-derived and conventional dendritic cells and reveals their distinct role during intramuscular immunization. *J Immunol* 188(4):1751–1760.
 37. Subramanian A, et al. (2005) Gene set enrichment analysis: a knowledge-based approach for interpreting genome-wide expression profiles. *Proc Natl Acad Sci USA* 102(43):15545–15550.
 38. Manicourt DH, et al. (2000) Synovial fluid levels of tumor necrosis factor alpha

- and oncostatin M correlate with levels of markers of the degradation of crosslinked collagen and cartilage aggrecan in rheumatoid arthritis but not in osteoarthritis. *Arthritis Rheum* 43(2):281–288.
39. Kawanaka N, et al. (2002) CD14+,CD16+ blood monocytes and joint inflammation in rheumatoid arthritis. *Arthritis Rheum* 46(10):2578–2586.
 40. Peng T, et al. (2009) Evasion of the mucosal innate immune system by herpes simplex virus type 2. *J Virol* 83(23):12559–12568.
 41. Thaïss CA, Levy M, Itav S, Elinav E (2016) Integration of innate immune signaling. *Trends Immunol* 37(2):84–101.
 42. Dorrington MG, Fraser IDC (2019) NF- κ B Signaling in Macrophages: Dynamics, Crosstalk, and Signal Integration. *Front Immunol* 10:705.
 43. Pandey S, et al. (2020) Pairwise Stimulations of Pathogen-Sensing Pathways Predict Immune Responses to Multi-adjuvant Combinations. *Cell Syst* 11(5):495–508.e10.
 44. Quintin J, et al. (2012) *Candida albicans* infection affords protection against reinfection via functional reprogramming of monocytes. *Cell Host Microbe* 12(2):223–232.
 45. Saeed S, et al. (2014) Epigenetic programming of monocyte-to-macrophage differentiation and trained innate immunity. *Science* 345(6204):1251086.
 46. Foster SL, Hargreaves DC, Medzhitov R (2007) Gene-specific control of inflammation by TLR-induced chromatin modifications. *Nature* 447(7147):972–978.
 47. del Fresno C, et al. (2009) Potent phagocytic activity with impaired antigen presentation identifying lipopolysaccharide-tolerant human monocytes: demonstration in isolated monocytes from cystic fibrosis patients. *J Immunol* 182(10):6494–6507.
 48. Karmaus PWF, et al. (2017) Critical roles of mTORC1 signaling and metabolic reprogramming for M-CSF-mediated myelopoiesis. *J Exp Med* 214(9):2629–2647.
 49. Lee PY, et al. (2017) The metabolic regulator mTORC1 controls terminal myeloid differentiation. *Sci Immunol* 2(11).
 50. Zhao Y, et al. (2018) mTOR masters monocyte development in bone marrow by decreasing the inhibition of STAT5 on IRF8. *Blood* 131(14):1587–1599.
 51. Smink JJ, et al. (2009) Transcription factor C/EBP β isoform ratio regulates osteoclastogenesis through MafB. *EMBO J* 28(12):1769–1781.
 52. O'Connell RM, Taganov KD, Boldin MP, Cheng G, Baltimore D (2007) MicroRNA-155 is induced during the macrophage inflammatory response. *Proc Natl Acad Sci USA* 104(5):1604–1609.
 53. Ceppi M, et al. (2009) MicroRNA-155 modulates the interleukin-1 signaling pathway in activated human monocyte-derived dendritic cells. *Proc Natl Acad Sci USA* 106(8):2735–2740.
 54. O'Connell RM, et al. (2008) Sustained expression of microRNA-155 in hematopoietic stem cells causes a myeloproliferative disorder. *J Exp Med* 205(3):585–594.
 55. Kurowska-Stolarska M, et al. (2011) MicroRNA-155 as a proinflammatory regulator in clinical and experimental arthritis. *Proc Natl Acad Sci USA* 108(27):11193–11198.
 56. Dunand-Sauthier I, et al. (2011) Silencing of c-Fos expression by microRNA-155 is critical for dendritic cell maturation and function. *Blood* 117(17):4490–4500.

57. Stanczyk J, et al. (2008) Altered expression of MicroRNA in synovial fibroblasts and synovial tissue in rheumatoid arthritis. *Arthritis Rheum* 58(4):1001–1009.
58. Elmesmari A, et al. (2016) MicroRNA-155 regulates monocyte chemokine and chemokine receptor expression in Rheumatoid Arthritis. *Rheumatology* 55(11):2056–2065.
59. Love MI, Huber W, Anders S (2014) Moderated estimation of fold change and dispersion for RNA-seq data with DESeq2. *Genome Biol* 15(12):550.
60. Malosse C, Henri S (2016) Isolation of Mouse Dendritic Cell Subsets and Macrophages from the Skin. *Methods Mol Biol* 1423:129–137.

Supplementary text

Supplementary Material and Methods

Flow cytometry of human monocyte-derived cells

Cells were stained for 30 minutes at 4°C with TruStain blocking solution (Biolegend), anti-CD16 FITC (BioLegend, clone 3G8), anti-CD1a APC (BioLegend, clone HI149), anti-CD1a PerCPy5.5 (BioLegend, clone HI149), anti-CD163 PE (BioLegend, clone GHI/61), anti-MERTK APC (R&D Biotechne, clone 125518), anti-CD88 PE (BioLegend, clone S5/1), anti-CD206 AF647 (BioLegend, clone 5-2), anti-CD226 PeCy7 (Biolegend, clone 11A8), anti-CD1b APC (ebiosciences, clone eBioSN13), anti-HLADR APC-eFluor 780 (eBiosciences, clone LN3), anti-CD86 PeCy7 (BioLegend, clone IT2.2), anti-CD40 V500 (BD Biosciences, clone 5C3), anti-CD80 PE (BD Biosciences, clone L307.4). DAPI (Fischer Scientific, 100ng/mL) was added immediately prior to acquisition.

Cytokine secretion

To assess monocyte activation, monocytes were cultured in RPMI (Gibco) supplemented with 10% FCS and antibiotics in the presence of M-CSF, IL-4, TNF- α and PRR ligands for 24h, and supernatant were collected. For the kinetics of TNF- α secretion, monocytes were cultured in RPMI supplemented with 10% FCS and antibiotics, in the presence of M-CSF, IL-4 and PRR ligands for 3, 6 and 24h, and supernatants were harvested. For the restimulation experiments, mo-DC and mo-mac were sorted on a FACS Aria instrument (BD Biosciences) following staining with anti-CD16 FITC and anti-CD1a APC and cultured for 24h in RPMI supplemented with 10% FCS and antibiotics, and supernatants were collected.

Western blot

Cells were lysed in RIPA buffer (Thermo Fisher Scientific) in the presence of cOmplete Mini EDTA-free protease inhibitor cocktail (Roche) at different timepoints. Proteins were separated by SDS-Page using a 4-12% BisTri NuPAGE gels (Bio-rad) and were transferred to membranes. Membranes were incubated with primary antibodies and then by secondary antibodies coupled to HRP (Jackson ImmunoResearch). Revelation was performed using Immobilon Forte Western HRP substrate (Millipore).

Reverse transcription quantitative PCR

Cells were lysed in RLT buffer and total RNA was extracted using the RNeasy microkit (Qiagen) according to the manufacturer's recommendations. Reverse transcription was carried out with Superscript II polymerase (Invitrogen) in combination with random hexamers, oligo deoxythymine and deoxynucleotide triphosphates. Quantification of the transcripts was performed on a LightCycler 480 instrument (Roche) using a master mix (Eurogentec) and the following Taqman Assays (Thermo Fisher Scientific): MAFB (HS00271378_s1), IRF4 (Hs_01056533_m1), MIR155HG (Hs01374569_m1). Housekeeping genes were: B2M (HS00187842_m1), HPRT (Hs02800695_m1), RPL34 (Hs00241560_m1) was quantified.

RNA-seq library preparation

Total RNA was extracted using the RNeasy minikit (Qiagen) including on-column DNase digestion according to the manufacturer's protocol. The integrity of the RNA was confirmed in BioAnalyzer using RNA 6000 Pico kit (Agilent Technologies) ($8.8 < RIN < 10$). Libraries were prepared according to Illumina's instructions accompanying the TruSeq Stranded mRNA Library Prep Kit (Illumina). 500 ng of RNA was used for each sample. Library length profiles were controlled with the LabChip GXTouchHT system (Perkin Elmer). Sequencing was performed in 4 sequencing unit of NovaSeq 6000 (Illumina) (100-nt-length reads, paired end) with an average depth of 40 millions of clusters per sample.

RNA-seq data analysis

Genome assembly was based on the Genome Reference Consortium (hg38). Quality of RNA-seq data was assessed using *FastQC* (1). Reads were aligned to the transcriptome using *STAR* (2). Differential gene expression analysis was performed using *DESeq2* using the design 'donor + group'. Genes with low number of counts (<10) were filtered out. Differentially expressed genes were identified based on adjusted p-value < 0.01 and Log₂ FoldChange > 0.5. Volcano plots were generated with *EnhancedVolcano* (3). Heatmaps of scaled expression were generated with *ComplexHeatmap* (4).

Flow cytometry of mouse cells

Cells were incubated with Zombie NIR fixable viability kit 15 minutes at 4°C (1/1000). Cells were then stained with anti-CCR2 BV711 (BD Biosciences, clone 475301), anti-CD11c BV786 (BD Biosciences, clone HL3), anti-CD26 PE (Biolegend, clone DPP-4), anti-CD3 BV480 (BD Biosciences, clone 17A2), anti-SiglecF BV480 (BD Biosciences, clone E50-2440), anti-CD19 BV480 (BD Biosciences, clone 1D3), anti-NK1.1 BV480 (BD Biosciences, clone PK136), anti-CD11b BV750 (BD Biosciences, clone M1-70), anti-MHCII BV650 (BioLegend, clone M5/114.15.2), anti-CD24 PeCy5 (BioLegend, clone M1/69), anti-CD226 PeDazzle594 (Biolegend, clone 10E5), anti-CD45 AF532 (eBiosciences, clone 30-F11), anti-Ly6G BV605 (BioLegend, clone 1A8), anti-CD64 PeCy7 (Biolegend, clone X54-5/7.1), anti-Ly6C AF700 (BioLegend, clone HK1.4), anti- EpCAM APCFire750 (BioLegend, clone G8.8), anti-CD11b PeCF594 (BD Biosciences clone M1-70), anti-CD45 FITC (BioLegend, clone 30-F11).

Data cleaning to select live CD45+ cells was done using FlowJo software then supervised analysis was performed on the same software.

For unsupervised data analysis, live CD45+ non-Langerhans cells (EpCAM-), non-neutrophils (Ly6G-) and non-T/B/NK/eosinophils (lin-) events were selected, extracted as new .fcs file for each sample and uploaded on OMIQ platform (<https://www.omiq.ai/>). Samples were downsampled to 4000 events per file and Uniform Manifold Approximation and Projection (UMAP)(5, 6), a non-linear dimension reduction algorithm, was used to visualize single cell data as 2D UMAP maps using phenotypic markers as parameters (Ly6C, MHCII, CCR2, CD11b, CD11c, CD24, CD26, CD64). For more advanced data visualization and exploration of spectral cytometry data, FlowSOM algorithm was used to identify cell subsets. FlowSOM uses Self-Organizing Maps (SOMs) to partition all individual cells based on their marker expression phenotypes into clusters and metaclusters (i.e., groups of clusters). In our study, number of identified metaclusters was determined automatically by the elbow metaclustering method based on the following markers: Ly6C, MHCII, CCR2, CD11b, CD11c, CD24, CD26, CD64, CD226.

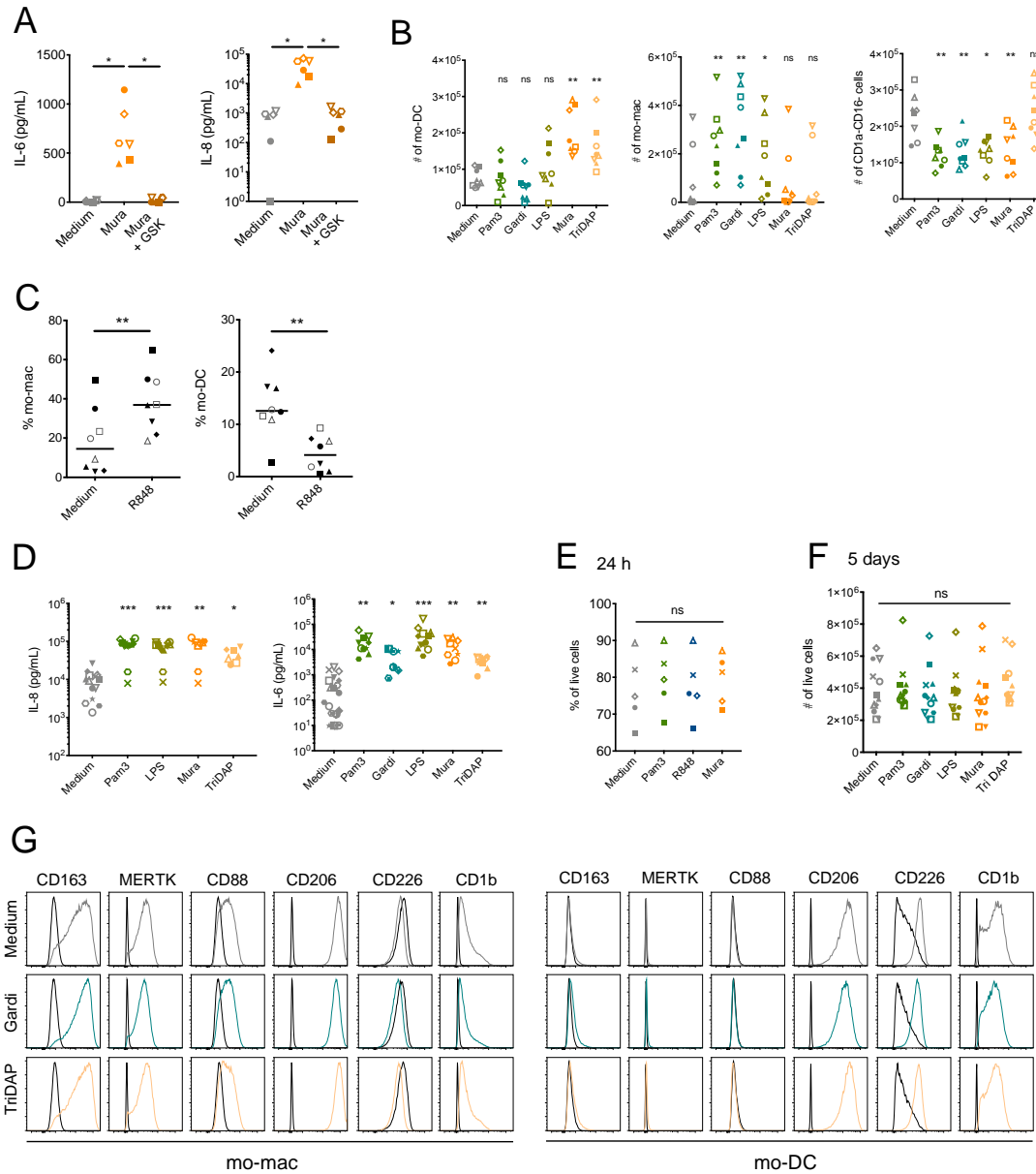


Fig. S1.

Pathogen sensing affects monocyte differentiation, but not their survival or the phenotype of mo-DC and mo-mac

(A) Monocytes were pre-incubated with 1 μ M GSK583 for 30 minutes, Murabutide was added and secretion of IL-6 and IL-8 was measured after 24h of culture (n=6). (B-G) Monocytes were cultured with M-CSF, IL-4 and TNF- α in the presence or absence of indicated TLR and NOD receptor ligands. (B) Total numbers of mo-DC, mo-Mac and undifferentiated cells after 5 days of culture in the presence of indicated ligands. (C) Percentages of mo-mac and mo-DC after 5 days of culture in the presence of R848 (n=8). (D) After 24h of culture, IL-8 (n>7) and IL-6 (n>6) secretion were measured. (E) Graph showing the percentage of live cells after 24h of culture (n=5). (F) Total number of live cells, mo-DC, mo-mac and undifferentiated cells was assessed after 5 days of culture using counting beads (n=12). (G) Expression of the surface markers CD163, MERTK, CD88, CD206, CD226 and CD1b was analyzed after 5 days of culture. Empty histograms correspond to isotype controls. Representative of 3 independent experiments. Wilcoxon test. *, P<0.05; **, P<0.01; ***, P<0.001. Mura=Murabutide, Gardi=Gardiquimod.

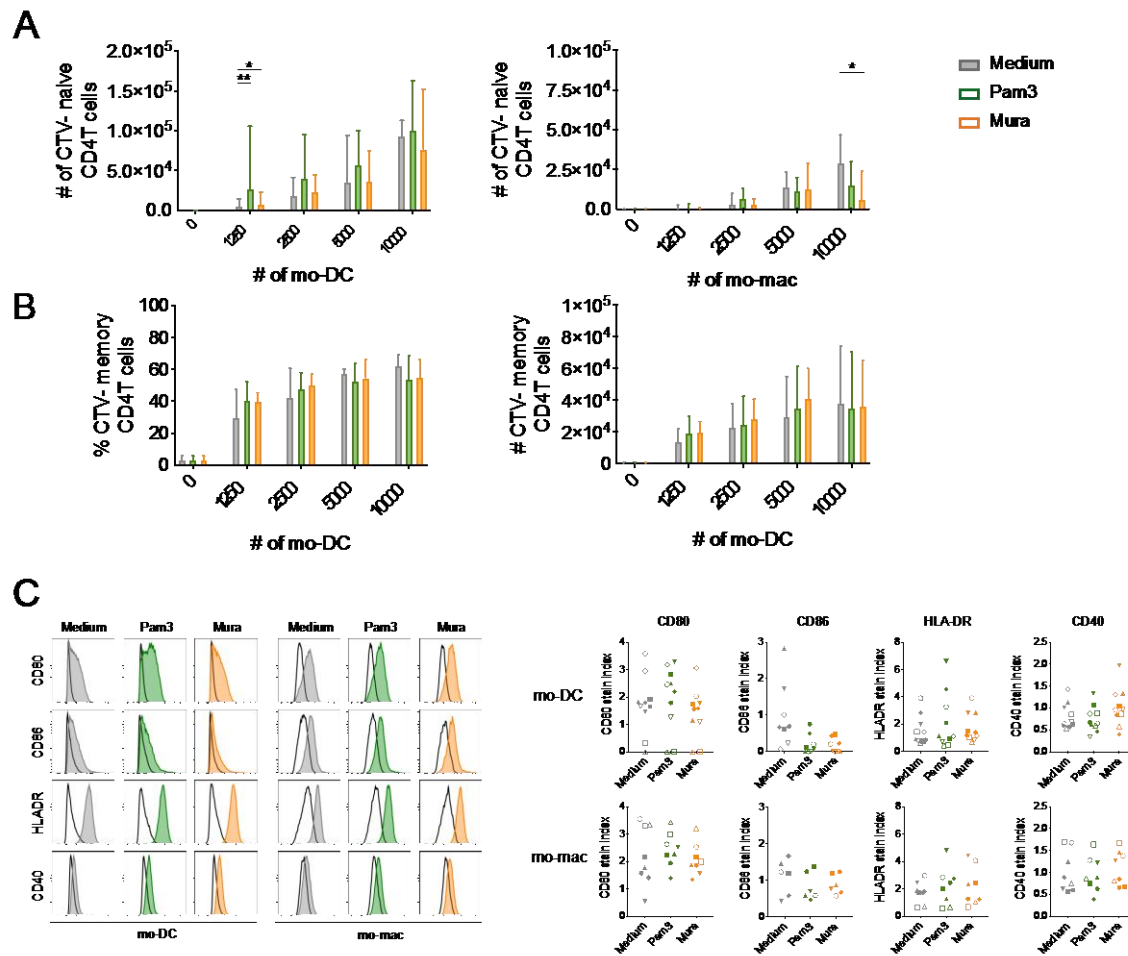


Fig. S2. Exposure of monocytes to Pam3 and Murabutide modifies the ability of mo-DC and mo-mac to stimulate naive CD4 T cell proliferation but not their expression of co-stimulatory molecules

Monocytes were cultured for 5 days with M-CSF, IL-4 and TNF- α in the presence or absence of Pam3 or Murabutide. (A-B) At day 5, mo-DC and mo-mac were sorted and co-cultured with blood allogenic naive CD4 T cells (A) or memory CD4 T cells (B) for 6 days. Proliferation of CD4 T cells was analyzed by measuring the dilution of a proliferation trace dye (CTV). Percentage and total numbers of CTV-cells are shown. The median and interquartile range are represented (n=6). (C) Expression of CD80, CD86, HLADR and CD40 was analyzed on mo-mac and mo-DC. Empty histograms correspond to isotype controls. Stain index for CD80, CD86, HLADR and CD40. Each symbol represents an individual donor (n>6).

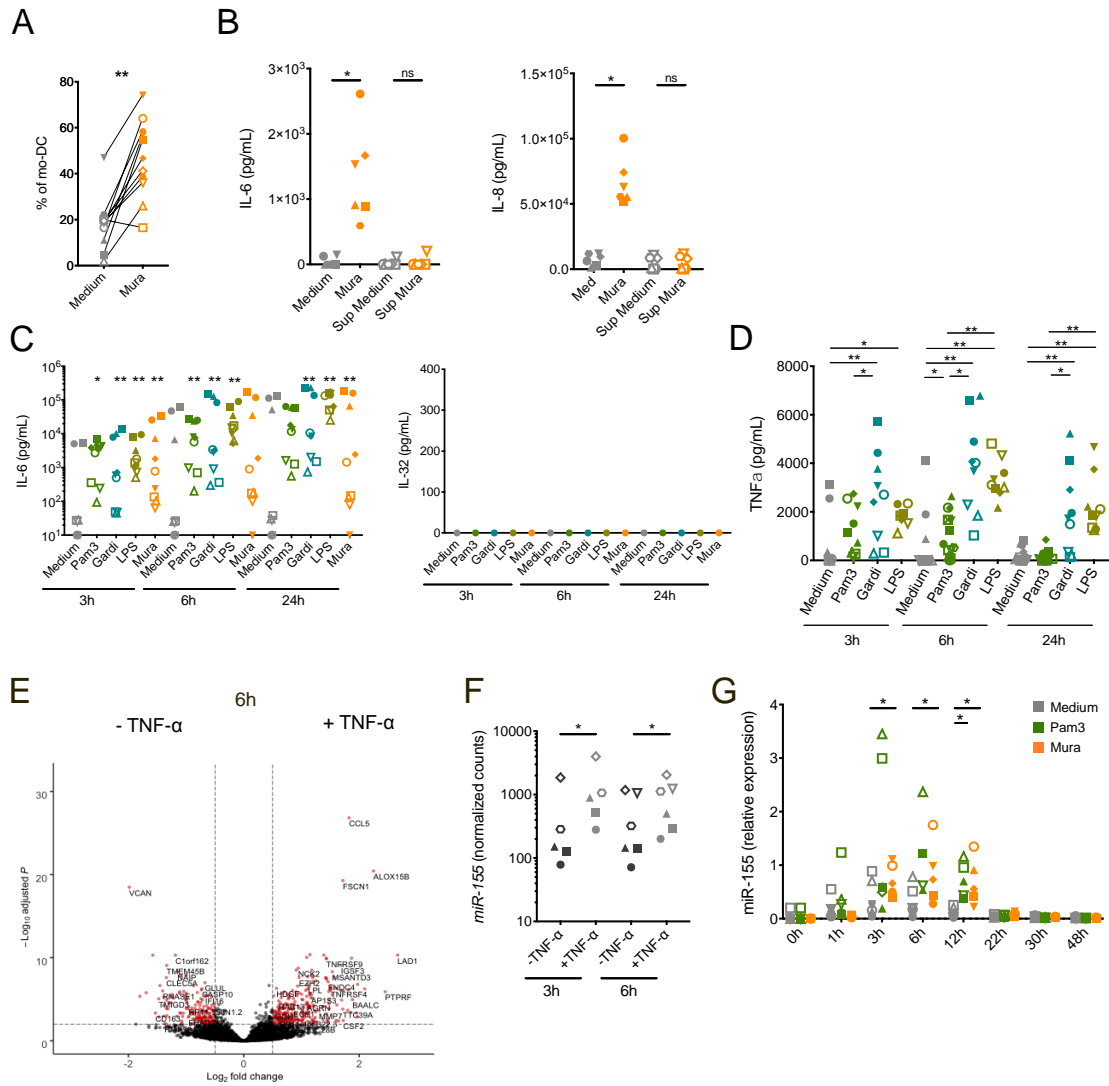


Fig. S3. Human monocytes secrete TNF- α but not IL-32 and upregulate miR-155 upon exposure to TLR and NOD receptor ligands

(A) Monocytes from the same donors that the ones used in the supernatant transfer experiments were culture for 5 days with M-CSF, IL-4 and TNF- α in the presence of murabutide. After 5 days of culture, monocyte differentiation was assessed by flow cytometry (n=11). (B) Overnight IL-6 and IL-8 secretion was measured in supernatants of monocytes activated or not by Murabutide, or in supernatants of monocytes that received the conditioned supernatant collected after 1 hour (n=6). (C-D) Monocytes were cultured with M-CSF, IL-4 and TNF- α and the indicated ligands. IL-6 (C) and IL-32 (C) and TNF- α (D) secretion was measured in supernatants after 3, 6 and 24 hours of culture (n=9). (E-F) Monocytes were cultured with M-CSF and IL-4 in the presence or absence of TNF- α for 6 hours and analyzed by RNA-sequencing (n=5). (E) Volcano plots showing differentially expressed genes in the presence of TNF- α versus control condition at 6h. (F) Normalized counts of miR-155. (G) Monocytes were cultured with M-CSF, IL-4 and TNF- α in the presence of indicated ligands. At different timepoints, mRNA expression of miR-155 was measured by RT-qPCR. Each symbol represents an individual donor (n>5). Wilcoxon test. *, P<0.05.

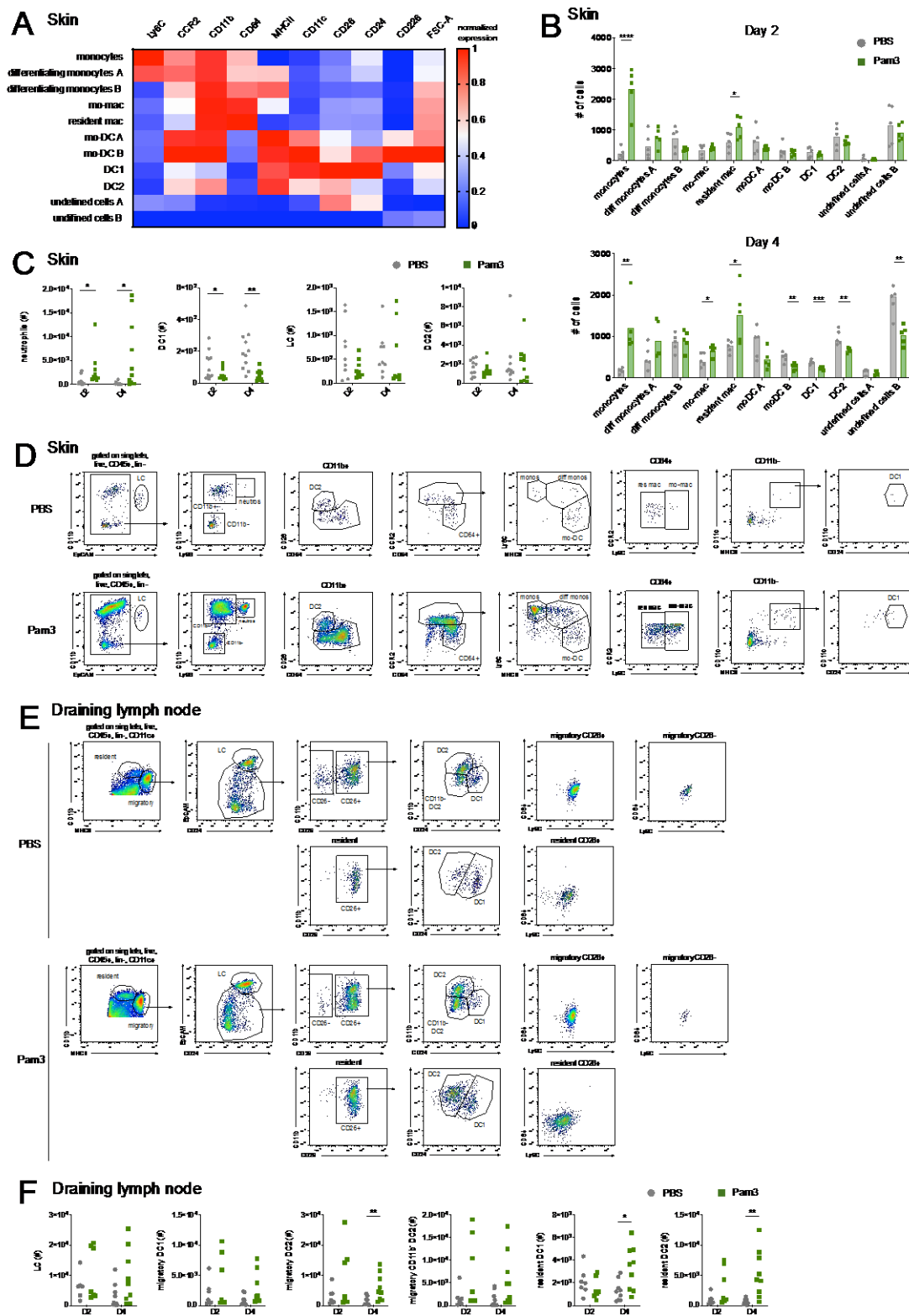


Fig. S4. Intra-dermal Pam3 injection increases mo-mac in mouse skin

Pam3 or PBS as control, was injected intradermally in ears of C57B6/J mice. (A-D) Single cell suspensions were prepared by mechanical and enzymatic digestion of each ear. (A) Heatmap of the normalized median expression of 9 myeloid markers for cell clusters identified by FlowSOM. (B) Number of cells in each cluster. Each symbol corresponds to an individual mouse (2 independent experiments). (C) Total cell numbers of neutrophils, DC1, LC and DC2 are represented based on the

manual gating strategy. Each symbol corresponds to an individual mouse (3 independent experiments). (D) Manual gating strategy. After exclusion of dead cells, doublets, CD45- and lineage+ cells, cells were separated into Langerhans cells (LC), neutrophils (neutros), monocytes (monos), differentiating monocytes (diff monocytes), mo-DC, mo-mac, resident macrophages (res mac), DC2 and DC1. (E-F) Single cell suspensions were prepared by mechanical and enzymatic digestion of ear-draining lymph nodes. (E) Manual gating strategy. After exclusion of dead cells, doublets, CD45- cells, lineage+ cells and CD11c- cells, cells were separated into Langerhans cells (LC), migratory DC1, migratory DC2, migratory CD11b- DC2, resident DC1 and resident DC2. (F) Total numbers of each population are represented. Each symbol corresponds to one individual mouse (3 independent experiments). Student T test. *, P<0.05; **, P<0.01; ***, P<0.001; ****, P<0.0001.

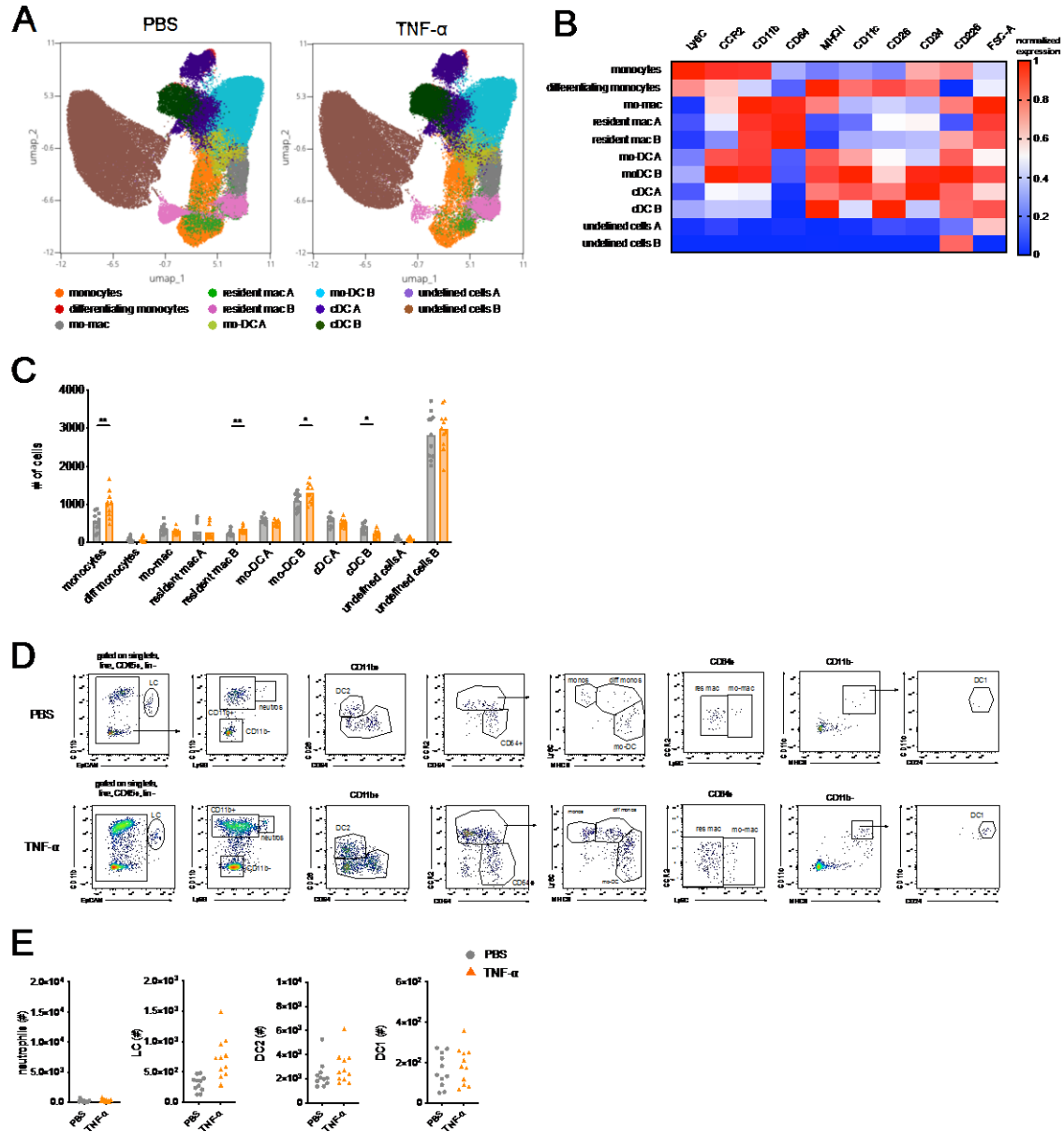


Fig.

S5. Intra-dermal TNF- α injection promotes mo-DC differentiation in mouse skin

TNF- α or PBS as control, was injected intradermally in ears of C57B6/J mice. Single cell suspensions were prepared by mechanical and enzymatic digestion of each ear. (A) UMAP representation of the 11 cell clusters identified by FlowSOM unsupervised analysis. Each dot represents an individual cell. Data is pooled from 11 individual mice in 3 independent experiments. (B) Heatmap of the normalized median expression of 9 myeloid markers for cell clusters identified by FlowSOM. (C) Number of cells in each cluster. Each symbol corresponds to an individual mouse (2 independent experiments). (D) Manual gating strategy. After exclusion of dead cells, doublets, CD45⁻ and lineage⁺ cells, cells were separated into Langerhans cells (LC), neutrophils (neutros), monocytes (monos), differentiating monocytes (diff monocytes), mo-DC, mo-mac, resident macrophages (res mac), DC2 and DC1. (E) Total cell numbers of neutrophils, LC, DC1 and DC2 are represented, based on the manual gating strategy. Each symbol corresponds to an individual mouse (3 independent experiments). Student T test. *, P<0.05; **, P<0.01; ***, P<0.001; ****, P<0.0001.

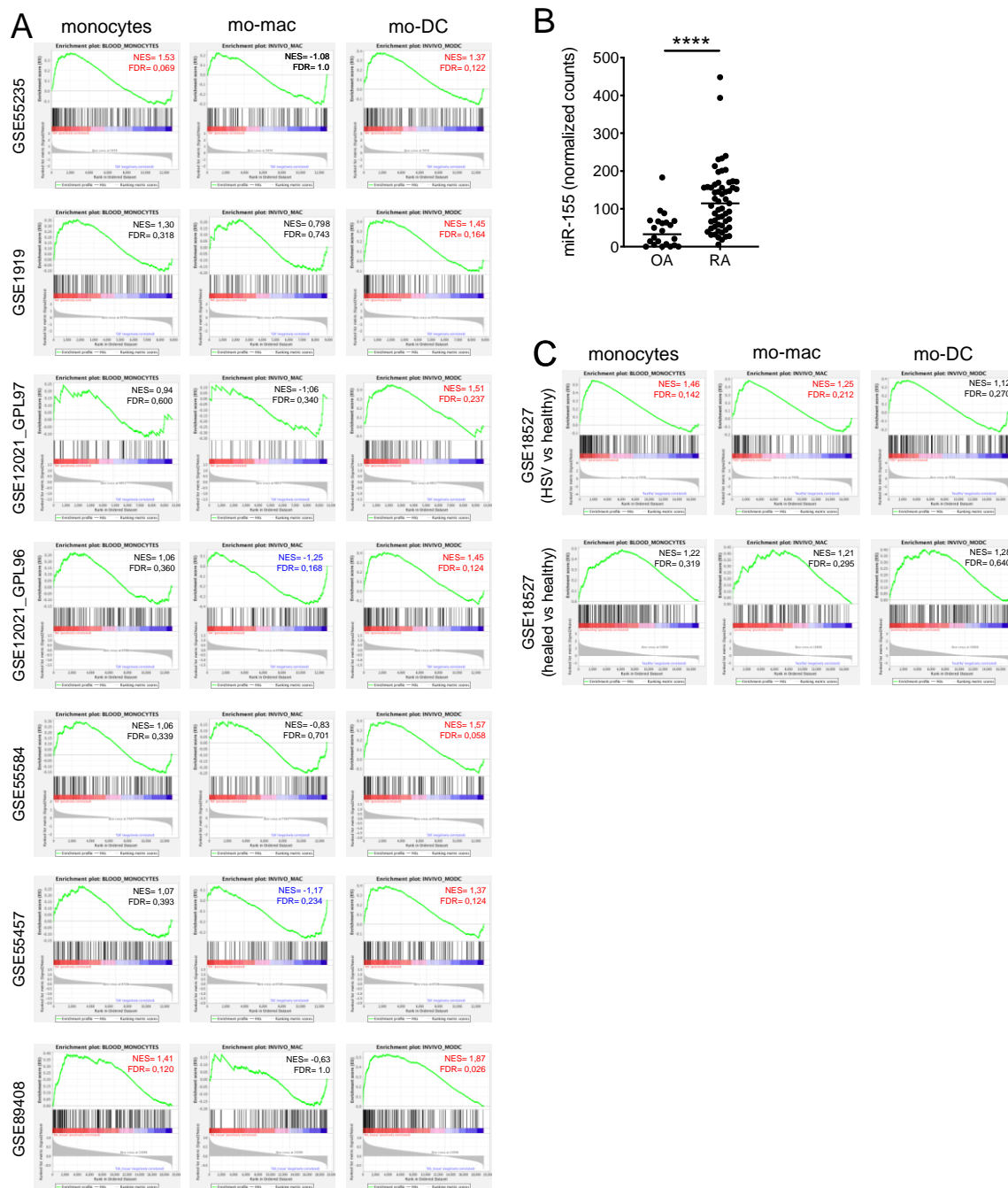


Fig.

S6. *In vivo* exposure to TNF- α or HSV-2 correlates with increased mo-DC or mo-mac differentiation in human biopsies

(A) Gene set enrichment plots for monocyte, mo-mac and mo-DC signatures on datasets from synovial biopsies from joints of rheumatoid arthritis or osteoarthritis patients. (B) Normalized counts for miR-155 in synovial biopsies from rheumatoid arthritis or osteoarthritis patients (GSE89408). (C) Gene set enrichment plots for monocyte, mo-mac and mo-DC signatures on datasets from skin biopsies from lesional or healthy skin of Herpes simplex virus 2 (HSV) infected patients during infection or after resolution. NES and FDR are indicated, in red or in blue depending in which datasets the signatures are enriched, or in black if there is no significant enrichment. Mann-Whitney test. ****, $P < 0.0001$.

SI references

1. Andrews S (2010) Babraham Bioinformatics - FastQC A Quality Control tool for High Throughput Sequence Data. Available at: <https://www.bioinformatics.babraham.ac.uk/projects/fastqc/> [Accessed February 16, 2021].
2. Dobin A, et al. (2013) STAR: ultrafast universal RNA-seq aligner. *Bioinformatics* 29(1):15–21.
3. Blighe K (2018) EnhancedVolcano. *Bioconductor*.
4. Gu Z, Eils R, Schlesner M (2016) Complex heatmaps reveal patterns and correlations in multidimensional genomic data. *Bioinformatics* 32(18):2847–2849.
5. McInnes L, Healy J, Melville J (2018) UMAP: Uniform Manifold Approximation and Projection for Dimension Reduction. *arXiv*.
6. Becht E, et al. (2018) Dimensionality reduction for visualizing single-cell data using UMAP. *Nat Biotechnol* 37:38–44.